Emissions Relationships in Western Forest Fire Plumes: I. Reducing the Effect of Mixing Errors on Emission Factors

Robert B Chatfield[1], Meinrat O Andreae[2 3], ARCTAS Science Team* and SEAC4RS Science Team*

[1] NASA Ames Research Center, Moffett Field, CA 94035, USA
[2] Max Planck Institute for Chemistry P.O. Box 3060, D-55020 Mainz, Germany
[3] Scripps Institution of Oceanography, UCSD, La Jolla, CA 92093, USA
* A full list of authors and their affiliations appears at the end of the paper.

Abstract: Studies of emission factors from biomass burning using aircraft data complement the results of lab studies and extend them to conditions of immense hot conflagrations. A new theoretical development of plume theory for multiple tracers is developed after examining aircraft samples. We illustrate and discuss emission relationships for 422 individual samples from many forest-fire plumes in the Western U.S. Samples are from two NASA investigations: ARCTAS (Arctic Research of the Composition of the Troposphere from Aircraft and Satellites) and SEAC4RS (Studies of Emissions and Atmospheric Composition, Clouds, and Climate Coupling by Regional Surveys). This work provides sample-by-sample enhancement ratios (EnRs) for 23 gases and particulate properties. Many EnRs provide candidates for emission ratios (ERs, corresponding to the EnR at the source) when the origin and degree of transformation is understood. From these, emission factors (EFs) can be estimated, provided the fuel dry mass consumed is known or can be estimated using the carbon mass budget approach. This analysis requires understanding the interplay of mixing of the plume with surrounding air. Some initial examples emphasize that measured $C_{tot} = CO_2 + CO$ in a fire plume does not necessarily describe the emissions of the total carbon liberated in the flames, C_{burn}. Rather, it represents $C_{tot} = C_{burn} + C_{bkgd}$, which includes possibly varying background concentrations for entrained air. Consequently, we present a simple theoretical description for plume entrainment for multiple tracers from flame to hundreds of kilometers downwind and illustrate some intrinsic linear behaviors. The analysis suggests a Mixed Effects Regression Emission Technique (MERET), which can eliminate occasional strong biases associated with the commonly used normalized excess mixing ratio (NEMR) method. MERET splits C_{tot} to reveal C_{burn} by exploiting the fact that C_{burn} and all tracers respond linearly to dilution, while each tracer has consistent EnR behavior (slope of tracer concentration with respect to C_{burn}). The two effects are separable. Two or three or preferably more emission indicators are required as a minimum; here we used eight. In summary, MERET allows fine spatial resolution (EnRs for individual observations) and comparison of similar plumes distant in time and space. Alkene ratios provide us with an approximate photochemical timescale. This allows discrimination and definition, by fire situation, of ERs, allowing us to estimate emission factors.

1. Introduction

1.1. Importance and previous work

Biomass burning has a large influence on the atmospheric burden of ozone and aerosols, and consequently also affects climate (Crutzen et al., 1979; Crutzen and Andreae; 1990; Jaffe and Wigder, 2012; Andreae, 2019). Biomass burning emission factors that are useful to drive photochemical models are most often estimated by one of two sampling techniques (Akagi et al., 2011). In the first approach, measurements on the ground close to an open fire or on laboratory fires that are controlled to approximate natural conditions, can provide the most detailed information on sources. The burning conditions can be readily assessed and fit into parameterizations of the emissions process, provided the correct mix of burn types typical of large fires can be estimated. It can, however, be difficult to mimic and safely sample truly intense flaming conflagrations. In the second approach, measurements made from aircraft, provides a much wider sample of different fires and emissions from different regions of a single fire. However, the estimates can be difficult to classify as simply “flaming” or “smoldering” or even as defined mixtures of just two types. Adjoining areas with fires in various stages of combustion can merge into the same plume, or remain relatively distinct. These questions of classifications related to the originating fires are addressed statistically in a succeeding paper, Chatfield and Andreae (2020).

This work presents a rationale for more mathematically thorough attention in estimation of emission relationships and emission factors in contrasting case studies, and uses such studies to develop an entraining plume theory for emissions relationships. Illustrations show that this theory gives intuitively reasonable results in some more complex situations. This theory suggests a statistical regression technique; a second methodology section then gives details of implementation given the complexities of atmospheric sampling. The result, a key “equivalent background” estimate, is then applied to quantify the atmospheric signal of fuel burned, approximately the sum CO_2+CO; this allows quantification of emission factors.

Since this work takes a complex path winding through observations, simple theory, examples of regression methodology, basic results, and finally emission factors, we offer this table of contents:

8. Estimates of emissions ratios: Two MERET examples
    8.1. MERET results for our two examples
    8.2. Table of several significant emissions
9. Conclusions
    9.1. Questions for future research

End material and References.

A further guide is given at the end of Section 1.

Let us introduce our view of enhancement ratios, emission ratios, and emission factors. Under appropriately defined circumstances, the amount of fuel carbon burned that is liberated to the atmosphere is the sum of carbon added to the ambient air in the form of all fire-originated gases and particles as a result of combustion: In deriving emissions factors, i.e., how much of a species is emitted per kg of biomass burned, it is usual to obtain the amount of carbon burned by taking the difference of the sum of excess mixing ratios, CO_2 + CO + other carbon-containing emissions, including aerosol particles. To an accuracy within ≳1.5 % (totals from the datasets we analyzed) to 3 % (Andreae and Merlet, 2001), carbon burned or C_{burn} is approximated by the excess (CO_2 + CO), as measured above a background concentration, C_{bkgd} (Andreae et al., 1988

$$C_{\mathrm{Burn}} = \Delta C_{\mathrm{Tot}} = \Delta \mathrm{CO_2} + \Delta \mathrm{CO} + \Delta \mathrm{CH_4} + \Delta(\text{particulate carbon}) + \Delta\ \mathrm{(O)VOCs}$$

approximated here ... $$C_{\mathrm{Burn}} = \Delta C_{\mathrm{Tot}} \approx \Delta \mathrm{CO_2} + \Delta \mathrm{CO} \qquad (1)$$

for graphics and theory... $$C_{\mathrm{Tot}} = x \qquad C_{\mathrm{Burn}} = x - x^0 = C_{\mathrm{Tot}} - C_{\mathrm{Bkgd}}$$

where the Δ's refer to the enhancement relative to pre-burn air, and (O)VOCs refers to the carbon content of volatile organic species, possibly oxygenated (O). In measurement situations, where frequent, accurate measurements of CH_4 and particulate *C* are also available, their inclusion could add <1% precision to the estimates. Analysis proceeds similarly including these terms. This work uses some algebra and graphics, so we introduce $x\ = C_{\mathrm{Tot}}$ and $x^0\ C_{\mathrm{Bkgd}}$

An Enhancement Ratio (EnR) for a species or property *j* with mixing ratio y_j is then $\mathrm{EnR}_j = \Delta y_j / \Delta C_{\mathrm{Burn}}$. We will use this term "enhancement ratio," EnR, in this paper. When EnRs are sampled prior to substantial atmospheric transformation (e.g., chemistry or particulate processes), they describe ERs. More on the relationships of EnRs, ERs, and EFs is found in the Supplementary Material (SM), "Note on EnRs and ERs". ER estimation constitutes the analysis of atmospheric samples that contribute to EF. Emission factors are defined relative to the amount of fuel burned and are derived from emission ratios by accounting for the concentration of carbon in the biomass burned and adjustment of units (Andreae and Merlet, 2001). Separate methods of land analysis are employed. EFs can be derived from ERs by

$$\mathrm{EF}_j = \mathrm{ER}_j \times \frac{MW_j}{MW_c} \times C_{\mathrm{BM}} \qquad (2)$$

where $\mathrm{ER_j}$ is the emission ratio of species *j*, MW_j and MW_c are the molecular weight of species j and the atomic weight of carbon, respectively, and C_{BM} is the carbon content of the dry biomass. We focus on improving methods of finding EnRs and ERs, which enable EF estimation.

One part of EF estimation concerns the amount of fuel consumed in fires, its carbon content, and the fraction liberated to the atmosphere (i.e., excluding char remaining on the ground); here we will focus on the other part of the question, which concerns the relationship of emitted compounds to the *C* liberated to the atmosphere. Many of the EnRs we calculate appear good candidates for EF estimates. One remaining task, making specific links of particular EFs to appropriate fire conditions for which they apply, requires individualized trajectories and fuel characterizations. This task, relating atmospheric signals of fuel burned to the details of the surface burning of carbon, is beyond reasonable treatment in this publication, which focuses on improving the understanding of airborne samples. It seems likely to us that uncertainties on the relation of area and fuel burned contribute more error to emissions estimates than those contributions of minor *C*-containing species in the plume that were described above.

There are other uses for EnRs that arise in understanding fire plumes, which revolve around the evolution of relatively fresh smoke plumes, e.g., the enhancement of ozone, peroxy acetyl nitrate, or other bound (not NO or NO_2) nitrogen species (Alvarado and Prinn, 2009, Alvarado et al., 2009; 2010, Jaffe and Widger, 2012). These also should have a direct relation to the fuel carbon burned and other properties such as burning conditions, fuel moisture, and fuel *N* content.

A complication arises from the fact that pre-burn/non-burn air may have various compositions, especially when we consider various sources for low-level inflow air, and especially air that is entrained in the smoke plume by the time of sampling. This is an important topic, which has been discussed in detail by Guyon et al. (2005) and Yokelson et al. (2013) and that we will focus on below.

Two special sampling intensives utilizing NASA's fully instrumented DC-8 aircraft allowed us to investigate forest-burning emissions. In June, 2008, the aircraft sampled a variety of fire plumes around California (Jacob et al., 2010; Singh et al., 2010; 20erw12; Hornbrook et al. 2011) during the California ARCTAS (Arctic Research of the Composition of the Troposphere from Aircraft and Satellites) intensive period. In a later part of the campaign, the DC-8 sampled in Northern Canada (Simpson et al., 2011); we excluded these plumes as representing different, more boreal, forest burn conditions. In 2013, the DC-8 made several samplings of forest fires in California and the Rocky Mountain West during SEAC4RS (Studies of Emissions and Atmospheric Composition, Clouds and Climate Coupling by Regional Surveys; Toon et al., 2015). We analyzed all of these fire plumes, but excluded samples east of 102 °W, which were mostly from agricultural fires. Our aim was to understand a variety of plumes, but limit variation to a single general category (temperate forest fires) as used for three-dimensional simulation models and geographical summaries.

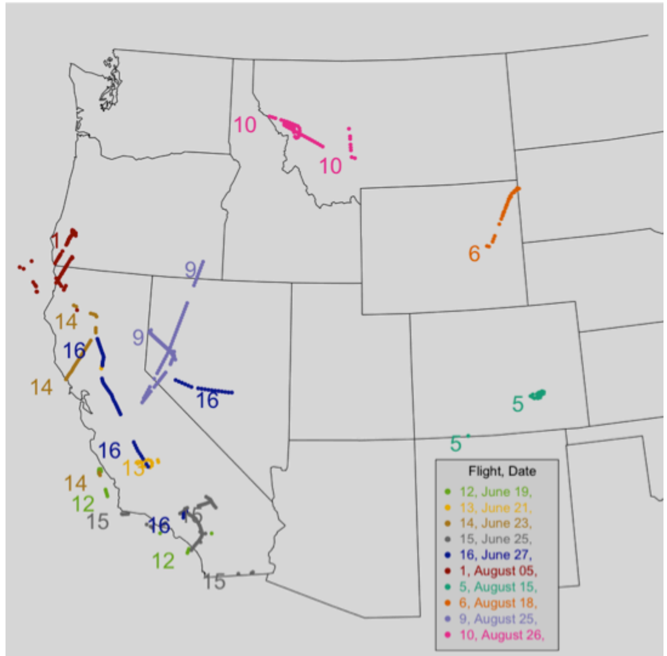

Figure 1. ARCTAS and SEAC4RS flights analyzed in this work. Each flight is identified by the flight number of that series. Flights 5 and 6 were in the Western US but not included.

Flight tracks for the period and locations of major fires during these periods are shown in Fig. 1. Analysis of the vertical variation of fire tracers suggested that plumes below 5 km ASL included recent and informative fires in our study. We saw no unequivocal variation of composition with height, possibly due to limitations on aircraft maneuvers low and near the fires. Consequently, the aircraft samples likely cannot adequately represent ground-hugging smoke flows.

1.2. Development of EF estimation to date

EnRs and EFs for biomass burning plumes have largely been based on measurements of the CO_2 or CO concentrations in the plumes. Typical analyses begin with measurements of C_{tot} and the concentrations of several tracers we may call y_j, $j = 1, \ldots N_{Tracers}$. Multiple instances $i = 1, \ldots N_{Instances}$ are observed, e.g., every few seconds or few minutes within a plume. An affine dependence (linear polynomial relationship including an intercept) is observed between each of the tracers and C_{tot} with a y-intercept that depends most significantly on the local out-of-plume background values of CO_2, CO, and each tracer individually.

$$C_{tot} = C_{bkgd} + C_{burn} \tag{3}$$

The following analysis suggests several complexities that must be addressed in order to understand these affine relationships. Several aspects of slopes, intercepts, and deviations from linearity of the relationship of tracer y_j to C_{tot} plots must be examined, and so we transition to graphic terminology with x representing C_{tot}. Later we will describe measurements of C_{tot} and tracers j at a given instance i, x_i and y_{ij}. For a simple plume within a homogeneous mixed layer characterized by an x concentration x^0 and y concentration y^E, we write

$$x = x^0 + (x - x^0) \tag{4}$$

and

$$\left(y_j - y_j^E\right) = a_j(x - x^0) \tag{5}$$

with enhancement ratios, a_j, that can yield ENRs directly. Early estimations (e.g., Greenberg et al., 1984; Andreae et al. 1988) used plots and regressions against CO_2 to estimate EnRs and EFs. These earliest techniques assumed fire was the main origin of CO_2. Very early it was recognized that other effects, e.g., variation of photosynthesis, respiration, and mixing required a more sophisticated approach (e.g., Guyon et al., 2005). Alternatively (e.g., Andreae et al., 1988; Hobbs et al., 2003; Lefer et al., 1994), EnRs were derived with respect to CO. Symbolically,

$$\text{EnR}\, Estimate = Estimate\overline{\left(\frac{\delta\, y_J}{\delta\,\text{CO}}\right)} \bullet Estimate\overline{\left(\frac{\delta\,\text{CO}}{\delta\,\text{CO}_2 + \delta\,\text{CO}}\right)}$$

= (Regression slope of y_i on CO) • (Regression slope of CO on (CO_2 + CO))

Here we use the symbol δ to indicate that these differences are evaluated from sequential samples or a regression of such a sequence. The second factor is based on the Modified Combustion Efficiency,

$$\text{MCE} = \delta\text{CO}_2/(\delta\text{CO}_2 + \delta\text{CO}) = 1 - \delta\text{CO}/(\delta\text{CO}_2 + \delta\text{CO}) = 1 - \text{EnR}_{\mathbf{CO}}\,. \tag{6}$$

with an attempt to estimate of the domain of points for which a constant MCE could be assumed. The form of the difference symbol is written as to emphasize that the differences are typically taken from a contiguous sampled time series of observations.

The method has become known as the normalized excess mixing ratios method (NEMR; Akagi et al, 2011). Yokelson and others (2013) described the care required to make sure that the MCE was well defined; otherwise, severe difficulties ensue. They describe a situation in which x^0 and y_{CO}^{E} in a diluting plume took on two distinct values, a mixed-layer value and a free-troposphere value, during plume rise and transport. More than two values may be relevant, emphasizing their call for a more thorough sampling of pre-fire air and its dilution environment. We describe below new methods to resolve many of the difficulties with x^0 and to indicate unwanted effects of y_{CO}^{E} variability. These methods could provide EnRs for many species with reasonable precision under more conditions.

This need for caution was very evident in the ARCTAS and SEAC4RS observational situations. Some Western USA data we analyzed showed variations in background C_{tot} = CO_2 + CO (away from direct recent effects of respiration and photosynthesis) of 15 ppm (interquartile Range of 4 ppm), while other Western USA regions showed variations of ~8 ppm (according to the analyses in this paper that we present later in Fig. 4). The contributions from fires were often comparable to this variation, ~2 – 40 ppm, mean ~6 ppm. Air flowed from the west into forest fires at low altitudes, or later diluted the smoke plume at intermediate levels. We could expect background air with a variety of histories of influence by photosynthesis (lower resultant CO_2) or respiration (higher CO_2), or urban-influenced air (higher CO_2). Low-level inflow air could have been mostly affected by local forests, farming, etc. Some of the most problematic situations tend to be associated with plumes sampled early in the day, when air from a nocturnal boundary layer — strongly enriched with respiration CO_2 — is mixed into the smoke plumes (Guyon et al., 2005). There could also have been substantial variations in C_{tot} due to intercontinental transport, the composition reflecting long-previous modification due to these same processes and to latitudinal gradients. Yates et al. (2011) reported and more fully referenced atmospheric sampling of Western air showing variations in CO_2 and also CH_4 and O_3. On the east side of the Pacific Anticyclone, the common pattern was for descent and horizontal shearing displacements, producing substantial C_{tot} variations in both horizontal and vertical directions (Barry and Chorley, 1998).

Previous analyses have been made for the ARCTAS data, by Simpson et al. (2011) for the large Canadian fires sampled and by Hornbook et al. (2011) for all fires. The Hornbook article usefully complements this paper by describing features and origins of the plumes sampled. Both groups described novel methods, but followed the traditional CO-emissions-ratio or NEMR methodology (Andreae et al., 1988; Hobbs et al., 2003; Akagi et al., 2011). Pfister et al. (2011) considered the emissions and transport of CO in the California ARCTAS samples. Analyses for the SEAC4RS fires have also been reported (Liu, 2018).

The following sections provide motivation for and understanding of an alternate approach to the description of EnRs and EFs, the Mixed Effects Regression Estimation Technique, MERET; in some cases, MERET and NEMR may form complimentary supporting views of plume emissions. Whereas NEMR depends on multiple measurements in the same plume in an understood environment, MERET is typically applicable to individual measurements of similar EnR-determining fire conditions across many different plumes. It does instead require several informative fire tracer species be measured simultaneously, not simply CO_2 or CO, as well as the tracer whose EnR is desired. It can also be used for good candidate EFs when the environmental history of the plume is not well characterized. It is applicable to any plumes encountered, without need for extensive measurement of that plume history.

The MERET technique attempts to use the simultaneous variability, sample by sample, of a large set fire tracer compounds and aerosol descriptors to find a single quantification, C_{burn}, of fire emissions, which it splits from C_{bkgd} such that the sum is C_{tot}. To do so, it must also ascribe a set of EnRs to the fire tracers, and recognize that these EnRs may vary from sample to sample in a limited way. The interplay of these estimates contributing to C_{burn} and EnRs for each observation appears daunting. Section 3 will graphically illustrate how strongly effects beyond fire emissions describe variations in C_{tot}; also how similar and informative are various tracers as graphed against C_{tot}. Section 4 will describe a theory of multiple fire emissions co-emitted from a fire based on familiar plume concepts, and give examples. The examples show the linearity of the theory that such simple approaches with a limited number of parameter estimates yield a reasonable approximation to more complex behavior. Sections 5 and 6 describe a mixed-effects regression algorithm based on plume theory. Section 7 provides a limited number of EnR estimates and describes graphically how flight segments describing similar emissions conditions can be identified.

2. Methodology: defining an indicator dataset

An initial task is the identification of tracers informative about burning and sampling rates. The technique we describe requires the measurement of $C_{\mathrm{tot}} \approx CO_2 + CO$ and several concentrations of emitted species or similar, extensive, properties of emissions (e.g., dried-airstream scattering coefficients, b_{scat}), which we will call *emission indicator species* or tracers. A set of indicator species was chosen for this publication to enable deriving relevant EnRs and to support our initial classification (e.g., flaming, smoldering, high-N fuel, etc.). It is important to have as many differently behaving emission indicator species as possible, as different indicators may respond differently to different fuels and fire intensities ("fire chemistries"), and such variations are usually not known before analysis. We favored indicator species with rapid sampling rates, so as to define C_{burn} for the maximum number of instances, but certain variables like CO, CH_4, and b_{scat} had special claims, as they can be maximally expressed in important types of fires. For our samples, methane and methanol showed significant idiosyncrancies. Their cumulative probability distribution differed from all other tracers: prominently very high concentrations and much higher positive skewness. We surmise that this behavior resulted from other prominent sources, e.g. cattle raising, or that very long distance transport and long lifetimes caused very great non-fire sources, like CO_2. It was convenient to use these same frequently measured indicator variables to define C_{burn} and also for classification of fire chemistries. For classification, we added intensive variables, essentially ratios that should be physically independent of C_{burn}.

The emissions indicator species that satisfied these requirements for both missions are shown in Table 1, along with references to the measurement techniques and observers. Only extensive quantities (proportional to C_{burn}) are used in this paper. CO_2 was measured by Stephanie Vay (ARCTAS) and Andreas Beyersdorff (SEAC4RS) using the AVOCET instrument (Vay et al., 2011). In examining EnRs for various species, we also use the organic aerosol (OA) measurements [Wagner et al., 2015]. ARCTAS and SEAC4RS data sites give full information, as instrumentation characteristics naturally vary somewhat between missions. (https://www-air.larc.nasa.gov/cgi-bin/ArcView/arctas, https://www-air.larc.nasa.gov/cgi-bin/ArcView/seac4rs?DC8=1)

Our techniques use algorithms that currently allow few missing observations among the variables. The sampling rates for emission indicators measured by PTRMS (proton-transfer ionization mass spectrometry) differed between the two aircraft missions. The SEAC4RS mission acquired suitably complete PTRMS-derived datasets at a once-per-minute rate, and this defined the data interval used for both datasets. Additionally, in SEAC4RS CO was measured only by (less frequent) can samples for the first flights prior to the Rim Fire of 26 August, and CH_4 was sampled only by cans for all flights. These are important species: CO is the most commonly used tracer for fire plumes because of its favorable plume-to-background concentration ratio and readily available measurement instrumentation. It is also used to define the MCE in much of the biomass-burning literature (Yokelson et al., 1996; Jaffe and Widger, 2011). Consequently, SEAC4RS imposed additional difficulties and processing. However, we judged it important to include SEAC4RS in a combined analysis to broaden the fire chemistries analyzed, as the Rim Fire was exceptionally large, hot, and well sampled.

The selection of fire plumes required some care. While CH_3CN is a highly specific tracer of fires (Singh et al. 2012), detailed analysis suggests that it is not the best quantitative tracer. (Further analysis suggested that CH_3CN has variable EFs, so it signals fires well, but does not quantify C_{burn} adequately.) Plumes were characterized by levels of CH_3CN above 0.225 ppb, over four times the assumed background of 0.054 ppb. Since some plumes are known to be quite low in gas-phase emissions, a few samples with lower CH_3CN mixing ratios, but with $b_{scat} > 2 \times 10^{-2}$ were allowed in. Plots of CH_3CN vs b_{scat} suggested that a linear combination of the two minimal conditions clearly separated a population of forest fire plumes from other high-particulate situations.

There were forest-fire plumes for which urban sources of CO and other fire tracers made attribution and quantification problematic, and so a further test based on CO was applied to exclude urban samples, using CO vs. CO_2 plots for the years 2008 and 2013 separately (Fig. 2). We used a $\Delta CO/\Delta CO_2$ ratio of <33 ppb/ppm to exclude plumes with excessive urban contamination. The figure suggests that some plumes with modest levels of urban influence remained and a few genuinely uncertain situations were excluded where fire might still have been dominant. Species with sources other than biomass burning and with lifetimes sufficiently long to allow regional mixing can pose difficulties somewhat similar to CO_2 variability, with solutions suggested in Section 8.2 and Chatfield and Andreae (2019). We noted some localized observations of perplexing, consistently negative $\Delta CH_4/\Delta C_{tot}$ relationships in the ARCTAS data (but not other species) and removed these observation instances. Such relationships were found close to seaports or oil-producing regions.

Table 1. Indicator Variables

Concentration / property	Abbreviation	Technique	Group	Reference
Extensive quantities	*Proportional to total burned material, as measured by* C_{burn} *:*			
Toluene	$C_6H_5CH_3$	PTRMS	Wisthaler	Wisthaler, et al. 2013.
Benzene	C_6H_6	PTRMS	Wisthaler	Wisthaler, et al. 2013.
Formaldehyde	HCHO	LAS	Fried	Fried et al., 2008.
Acetonitrile	CH_3CN	PTRMS	Wisthaler	Wisthaler, et al. 2013.
Absorption Coefficient Dry, Total, 532 nm	b_{abs} , Abs_5	Nephelometry	Anderson	Wagner et al., 2015, Anderson Langley Aerosol Group, LARGE
Scattering Coefficient, Dry, Submicron 550 nm	b_{acat} , Scat_5	Nephelometry	Anderson	Wagner et al., 2015, Anderson Langley Aerosol Group, LARGE
Carbon monoxide	CO	LAS, GC	Diskin, Blake	Pfister et al., 2011.
Acetaldehyde	CH_3CHO	PTRMS	Wisthaler	Wisthaler, et all. 2013.
Intensive quantities	*Not proportional to carbon burned*			
Single Scattering Albedo	SSA	Nephelometry	Anderson	Wagner et al., 2015, Anderson
Ångström Exponent, scattering	ÅE	Nephelometry	Anderson	Wagner et al., 2015, Anderson
Other variables used	O_3, $NO_x = NO + NO_2$, NO_y	Chemilumines-cence, UV	Weinheimer (ARCTAS) Ryerson (SEAC4RS)	Weinheimer, et al. et al. 1994. Ryerson et al., 2000
Methane	CH_4	LAS, GC	Diskin, Blake	Pfister et al., 2011.
Methanol	CH_3OH	PTRMS	Wisthaler	Wisthaler, et al. 2013.

Notes: PTRMS: proton transfer mass spectrometry, LAS: laser absorption spectrometry. $1-\varpi$ is the single-scatter co-albedo: likewise, CO is linked to 1 – (Modified Combustion Efficiency), so that all values extend upwards from 0. CO_2 measurements: see text.

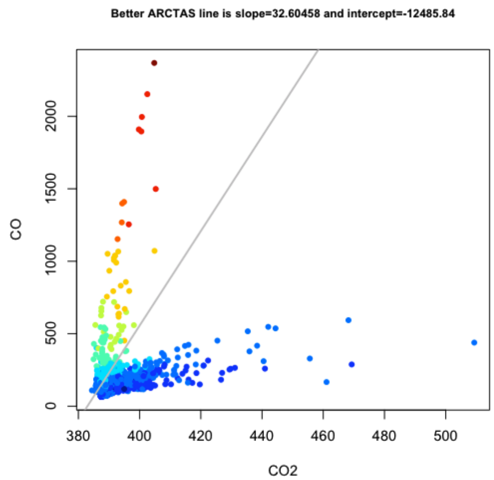

Figure 2. Urban and forest fire plumes are separable by the ratio of CO to CO_2. Colors indicate a relative measure of CH_3CN above background, from blue (lowest, ~0.1 ppb) to red (highest, ~6 ppb) values. The straight gray line indicates our selected discrimination between non-urban and urban.

3. Observed behavior of C_{tot} in fire plumes – Properties of tracers

This section provides some examples of C_{tot} and fire tracers. It illustrates the limitations of changes in C_{tot} along a sampling path as an indicator of fire influence, C_{burn}, for emissions estimation and the much greater similarities of the variations of tracers that possess shorter transformation time-scales. These define our approach to EnRs and EFs. The relation of fire emissions to observed C_{tot} to C_{burn}, can be apparently simple or complex, depending on how the history of non-fire CO and CO_2 entrained into fire plume air parcels affects C_{tot}. We show this commonality of relationships will to motivate the theory of expanding plumes in Section 4. The theory suggests a regression relationship in Section 5 and 6, which applied, yields results in Sections 7, that define relatively precise estimates of C_{bkgd}, C_{burn} and thus EnRs.

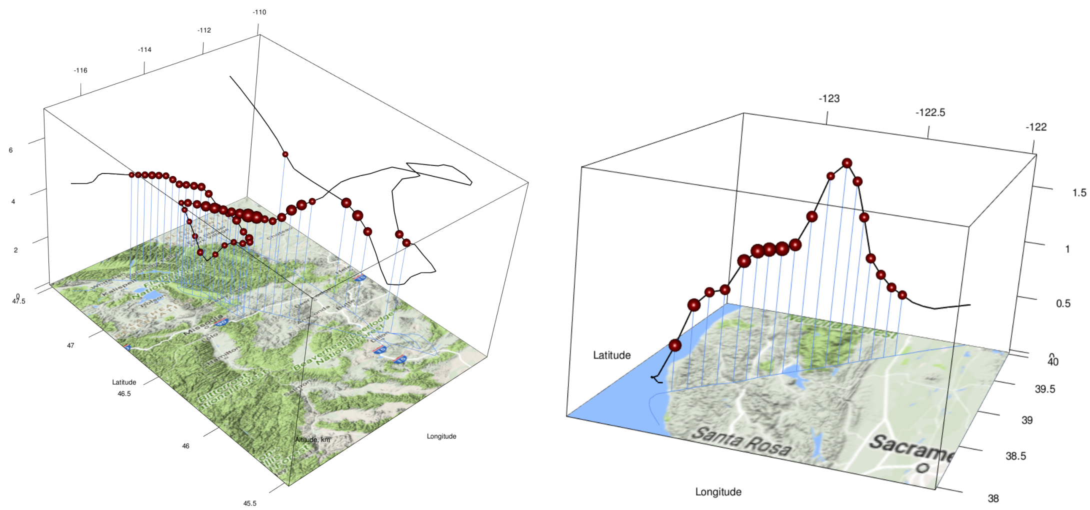

Figure 3. Flight paths and locations of plumes for two fire samples. **(a)** Sampling over Montana during SEAC4RS Flight 10. **(b)** Sampling in a cross-mountain transect along the Northern California Coast. The size of the spheres indicates the relative amount of biomass burning contribution. Numerical values of the contribution are in a later figure, Fig. 10. Some of the information was converted from GoogleMaps® using the R programing language.

Figure 3 describes two flights in which plume encounters show how the interpretation of $C_{\mathrm{tot}} = C_{\mathrm{burn}} + C_{\mathrm{bkgd}}$ can be simple or complex. Fig. 3a shows the locations of the plume samples observed during SEAC4RS Flight 10 over Montana between 2 and 4.5 km MSL. Local topography ranged from 1 to 2 km elevation. This data set included samples from the very intense plume of the Rim Fire (discussed later), collected far downwind. Figure3b shows ARCTAS Flight 14, which was over the Coastal Mountains of Northern California at 0.5 to 1.5 km altitude, with topography from 0 to 1 km.

Figure 4a (whose sampling path is mapped in Fig. 3a) gives the time series of fire indicators from Flight 10. The fire tracers CO and b_{scat} appear generally well correlated with C_{tot}. This correlation is seen in Fig. 4b-c. Colors from blue to red give a key to sampling times. The large orange dots in Figs. 4a and 4d distinguish the plume points *selected* (based on our plume tracers) from adjacent non-plume measurements made in the flight. The lines connecting the adjacent plume samples suggest two or perhaps three linear patterns pointing back to a no-fire background of $C_{\mathrm{tot}} \sim 392.5$ and 394.5 ppm. Separately, a few points near the horizontal axis seem to suggest a low EnR. These points occur in the middle of sampling, just after 11 LT. Patterns of variation related to b_{scat} (550 nm, Fig. 4c) are very similar to those of CO Fig. 4b. Most plumes encountered suggest very similar slopes.

Whereas the SEAC4RS Figs. 4a-c suggest mostly expected behavior, the ARCTAS Flight 14 measurements (Figs. 4d-f) show that C_{tot} variations, likely due to C_{bkgd} variability, can greatly complicate the attempt to estimate EnRs. The very first samples plotted and those after about 13:35 LT have very clean tracer levels. (Those between 13:03 and 13:15 LT did not quite qualify as plume points, but the tracers do indicate some fire influence.) In this case, the trace of C_{tot} does not reflect fire influence well at all. Both fire tracers shown in Figs. 4d-f show wildly varying relationships to C_{tot}, but are remarkably similar in that relationship.

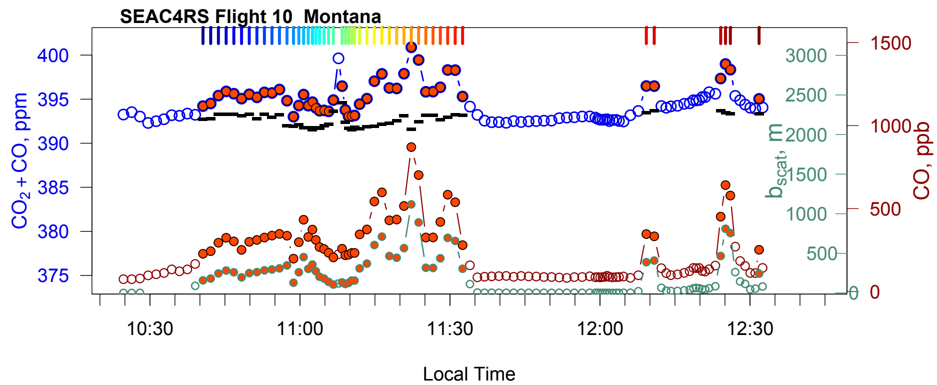
SEAC4RS Flight 10 Montana
$CO_2 + CO$, ppm
b_{scat}, m
CO, ppb
Local Time

(a)

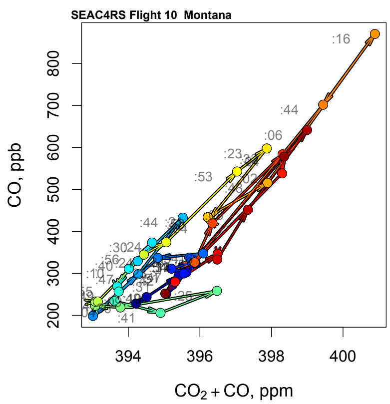
SEAC4RS Flight 10 Montana
CO, ppb
$CO_2 + CO$, ppm

(b)

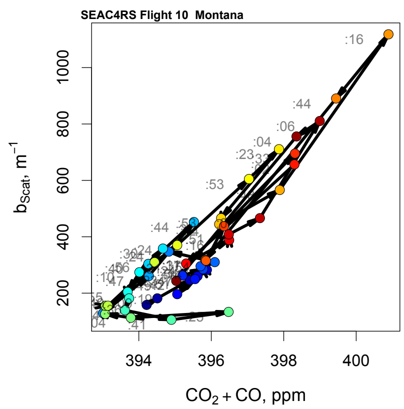
SEAC4RS Flight 10 Montana
b_{Scat}, m^{-1}
$CO_2 + CO$, ppm

(c)

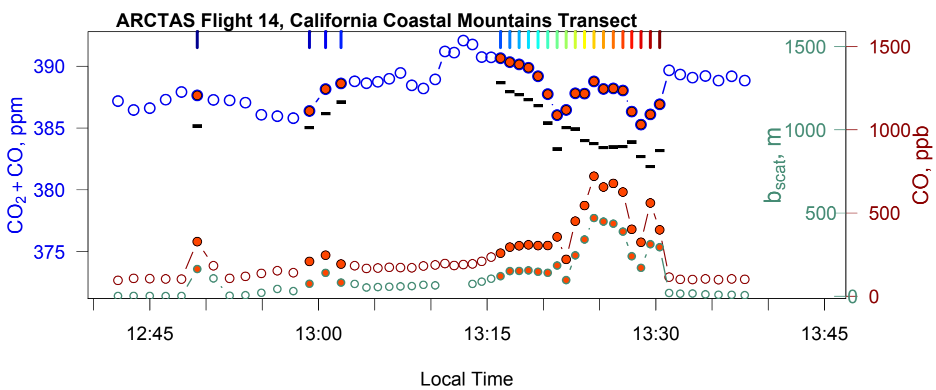
ARCTAS Flight 14, California Coastal Mountains Transect
$CO_2 + CO$, ppm
b_{scat}, m
CO, ppb
Local Time

(d)

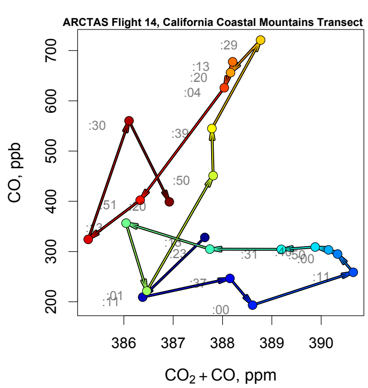
ARCTAS Flight 14, California Coastal Mountains Transect
CO, ppb
$CO_2 + CO$, ppm

(e)

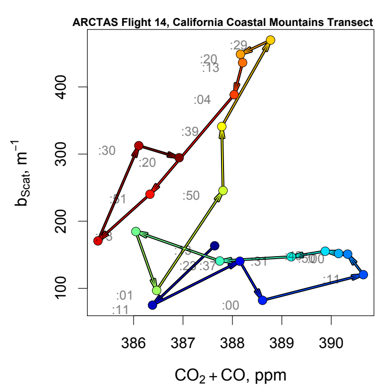
ARCTAS Flight 14, California Coastal Mountains Transect
b_{Scat}, m^{-1}
$CO_2 + CO$, ppm

(f)

Figure 4. (a) Timeline of sampling, for the period shown in Fig. 3a, Montana, of CO_2+CO (blue, left axis) and the fire tracers CO and b_{scat} (red and green points, right axis). Orange-filled points were identified as clear plume points. Unfilled points were not, but might have some fire influence, especially near plume points. **(b)** scatter diagram of CO vs CO_2+CO with arrows showing the time progression of aircraft sampling of identified plume points. Colors provide a key to times shown in (a). Light gray numerals give observation times in minutes. **(c)** a similar diagram of b_{scat} vs CO_2+CO. Similar shapes of figures are noted in the text. **(d)** Timeline of sampling for the period shown in Fig. 3b, Coastal Transect. **(e)** scatter diagram of CO vs CO_2+CO during the transect, like (b). **(f)** a similar diagram of b_{scat} vs CO_2+CO for the Coastal Transect. The black bars graphed in (a) and (d) are estimates of non-fire influenced C_{bkgd}, see text. They and the non-plume points suggest air-mass changes in CO_2+CO.

To conclude this section, we emphasize that variations in C_{bkgd} do occur unexpectedly in many apparently homogeneous datasets. The lines composed of small black bars in both Fig 4a and Fig 4d use our results of Section 7; they are estimates of C_{bkgd} for the selected fire-plume cases. The following patterns in Fig. 4 are given as plausible descriptions; the aim of this work is to support these with a uniform theory. For example, C_{tot} sampled by the airplane increases due to higher non-fire C_{bkgd} from just before 13:00 to 13:15, and then decreases gradually until about 13:28. At one sample around 13:21 and several at 13:20–13:30, the background is particularly low, 382–383 ppm. This is a plausible description of the mixing of air-masses with originally concentrations of C_{tot} ~382 and ~388 ppm. Wisps of less-mixed air occasionally interrupt a relatively continuing trend. A close examination of the CO and b_{scat} increments compared to C_{tot} increments in Figures 4d-4f agrees with this description suggested by the black dashes. The simpler case of SEAC4RS Flight 10 shows a similar example. At 11:08 LST, early in the flight, there is a brief excursion upwards of C_{tot} without any excursion in the tracers. The small black bars show this as a plausible excursion of C_{bkgd}. Figures 4b and 4c show this as the 2–3 exceptional points, colored green, near the horizontal axis.

The plausibility of these examples highlights ideas of fundamental similarities of the way plumes of different tracers behave with entrainment even as C_{bkgd} varies in response to distant, unrelated processes, as seen in Fig. 4a. This leads us to a mathematical description of our observations in Section 4.

4. Theory: expanding plume for several species

4.1. A general relationship

Figure 5 gives a general description of the dilution process, showing by the size of cubes how a mole of near-flame air is diluted by non-fire material as entrainment occurs. (The boxes shown suggest volumes, but lofting adiabatically changes volume. Discussion in terms of moles simplifies the discussion of mixing ratios and EnRs.) The figure is based on observations of plume size and plume dilution during rise followed by largely horizontal dilution downwind (Lareau et al., 2017; Hanna et al., 1982), which are consistent with mixing ratios measured in this dataset and near-fire CO_2 concentrations of 1–2.5 x 10^4 ppm. The sizes are meant to be suggestive, but we found that they give a valuable frame of discussion of all lofted forest fire plumes. Some details are in Supplementary Material (SM): "Note on Volumes."

Using Fig. 5 as a guide, consider a parcel originating at a time t_1 containing $\nu = \nu_1$ moles, that expands with an exponential relative rate $r_\nu = \nu^{-1}(d\nu/dt)$. (For our illustrative examples and to rationalize the MERET method, we need not start at the flame. We suggest a reasonable starting point described below.) This rate of expansion $r_\nu(t)$ of the molar volume varies considerably over time and fires are expected to have different magnitudes. Then molar mixing ratios will evolve with a law

$$\frac{dx}{dt} = -\frac{1}{\nu}\frac{d\nu}{dt}(x - x^E) \tag{7a}$$

$$\frac{dy_j}{dt} = -\frac{1}{\nu}\frac{d\nu}{dt}(y_j - y_j^E) \tag{7b}$$

where x^E is the mixing ratio of entraining C_{tot} and y_j^E is the entraining background mixing ratio of fire tracer species or property *j*. (The term x^E here is later called x^0 with a more general significance for possibly varying entrainment behavior.) The effect of volume addition is captured by $\nu(t)$ which varies with time and expansion. The use of the relative rate $\nu(t)$ does not require that the dilution is exactly exponential, but does make the algebra somewhat simpler.

Figure 5. Inflow of air into an expanding fire plume; a likely near-fire aircraft sampling location would be near the cube on the upper right. Cubes are shown with three-d sizes proportional to the number of moles of entrained air. These may be considered volumes of air adjusted downward to compensate for the adiabatic expansion that rising plumes undergo. The smallest cube is taken to be near the flames, at roughly the point where fire emissions transition from mixing to entraining background air. Exact placement of this cube is not important to the analysis of entrainment, expansion, and tracer mixing ratio. Successively larger cubes have volumes roughly in the ratio of 1, 40 (partially raised), 140 (near neutral buoyancy level); sizes are consistent with a buoyant fire plume (Lareau et al., 2017). The rightmost cube has a ratio to the first of 400, consistent with horizontal Gaussian dispersion during travel downwind. See text for more details.

What happens when there are variable values of $x^E(t)$ from fire to sampling point, for example boundary layer and free troposphere? Using τ to describe the integration through time of an expanding parcel,

$$y_j(t_{Sample}) = \int_0^{t_{Sample}} -\nu(\tau)\left(y_j(\tau) - y_j^E(\tau)\right) d\tau + y_j(t = 0) \tag{8}$$

with a similar equation for C_{tot}, which we can be called $x(t_{Sample})$. It involves $x(\tau)$ and $x^E(\tau)$ where $x(t=0)$ and $y_j(t=0)$. These are determined by the C_{burn} from the fuel consumed and the tracer compounds released at the same time, as well as background concentrations, C_{bkgd}, and pre-flame backgrounds of the tracer y_j^E. We leave aside as a separate problem for a fire-burning model the complexities of the actual flame and its incorporation of additional air. Our point $t = 0$ is when entrainment of non-burning air becomes dominant.

Given the realities of atmospheric sampling, we must avoid describing the complete history of $\nu(\tau)$ and any complex variation of $x^E(\tau)$ and $y_j^E(\tau)$. These would require a complete description of air along the parcel trajectory and the turbulent physics of entrainment. Rather, we provide simple illustrations showing how generally the entrainment process affects both $x(\tau)$ and all the $y_j(\tau)$ in the same proportions. This is a single-parcel description ignoring complexities of the rest of the plume. For convenience of discussion, we will describe cases in which the environmental air entrained has one or two values $x^E(\tau)$ and $y_j^E(\tau)$ constant over long periods. For example, it is constant in the mixed layer surrounding the fire flames and initial plume and then again in the subsequent regions often in the free troposphere. Conceptually there may be several regions which contribute; the exact history is lost. Our idea is that regression analysis allows us to infer a characteristic sum of effects which is described by a single quantity. The analysis can only be as complex as the number of our measured quantities allows. See also SM for Note on Initial Point.

Returning to the differential-equation view of the simple expanding plume model, we see a method for estimating the most important parameters. Solving each of the equations for the expansion rate and equating the expressions we obtain a form that eliminates the details of entrainment and emphasizes proportionality. We recommend the reader refer back to Table 2, Table of Symbols during the discussion of theory and then estimation details.

$$\frac{1}{(y_j - y_j^E)}\frac{dy_j}{dt} = -\frac{1}{\nu}\frac{d\nu}{dt} = \frac{1}{(x - x^E)}\frac{dx}{dt} \tag{9}$$

Since $dy_j^E/dt = 0 = dx^E/dt$, we get

$$\ln(y_j - y_j^E) = \ln(x - x^E) + C_j \tag{10}$$

$$(y_j - y_j^E) = a_j\,(x - x^E) \quad a_j = \exp\,(C_j) \tag{11}$$

Note that by our definitions, the reasonable interpretation of C_j is the EnR a_j for species j. Consider two observations of the same plume, each made at differing degrees of dilution ν. For convenience, these are labeled β and α, mnemonically "before" and "after." Temporally they could be nearly coincident or β after α,

$$(y_{\alpha j} - y_{\beta j}) - (y_j^{E\alpha} - y_j^{E\beta}) = a_j\,(x_\beta - x_\alpha) - a_j\,(x^{E\alpha} - x^{E\beta}) \tag{12}$$

For periods of expansion in which the entrained concentrations are constant. See also SM: Note on Varying Entrainment.

Table 2. Table of Symbols

Symbol	Signifies	*Observed, Estimated, or Hypothetical*
C_{tot}	CO_2 + CO (+ other carbon, ignored here), ppm.	*O*
C_{burn}	CO_2 + CO (+ other carbon, ignored) emitted from fire, present downwind, in plume sample, to be estimated as $(x_i - x_i^0)$).	*E*
C_{bkgd}	CO_2 + CO ***not*** emitted from fire, present downwind in plume sample, thought of as a mixture of C_{tot} entrained at various stages in plume expansion and rise. The background may be assumed for illustration, or computed from the estimated x_i^0. This is not necessarily air surrounding the plume sample.	*E* *H**
$C_{\mathrm{bkgd}}^{\mathrm{Approx}}$, v_i	Early approximate C_{burn}; a rough rescaling from the unitless burn-normalizing variable v_i to ppm, often a convenient guide and check.	*E*
C_j	A constant of integration, replaced by $a_j = \exp(C_j)$.	*H*
i	Sample sequence number, organized for convenience by time of the sample.	*O*
j	Tracer number for regression, om this work, 1 to 8, or "CO" or "b_{Scat}", … . After regression estimation is completed, j may be used similarly to specify any fire emission concentration or response, e.g. "propene" or "O_3".	*O*
a or b	Location at beginning or end of a period of idealized plume development and entrainment.	*H**
x_i	C_{tot}= CO_2 + CO at a plume sample location and time, used in algebraic development, shown on *x* axis.	*O*
y_{ij}	Tracer concentration, e.g. toluene, b_{Scat}, at plume location and time.	*O*
x^{E} or $x^{E\alpha}$	Environmental air "background" C_{tot} concentrations existing at location A, e.g. beginning of our integration of the plume expansion equation. B signifies condition at the end of calculation.	*H**
y_j^E or $y_j^{E\alpha}$	Background concentration of tracer *j* . Typically estimated as a minimum value from observed probability density function for samples in a particular flight intensive, especially non-plume samples without signals of stratospheric air.	*E*
a_j	Slope relationship of y_{ij} to x_i for species *j,* typically species *j* under burning conditions for a "fire type" that is common for all species at instance (time) i . These slopes then transform to EnRs and ERs.	*E*
c_j	Intercept relationship of y_{ij} to x_i.	*E*
y_{ij}^0	y intercept implied by x_i , y_{ij} and the estimated slopes a_j for *j.*	
$\hat{x}_{ij}^0$	One of several (10) estimates of x_i^0 based on tracer *j* and fire type assigned by clustering for observation instance i .	*E*
$\hat{x}_i^0$	The median of the $\hat{x}_{ij}^0$ over all the tracers *j.*	*E*
$(x_i - x_i^0)$	The estimate of C_{burn} for instance *i* in theoretical development and then from regression. Regression results are properly $(x_i - \hat{x}_i^0)$	*E*

Note that symbols may transition from Hypothetical to Estimated as the discussion develops.

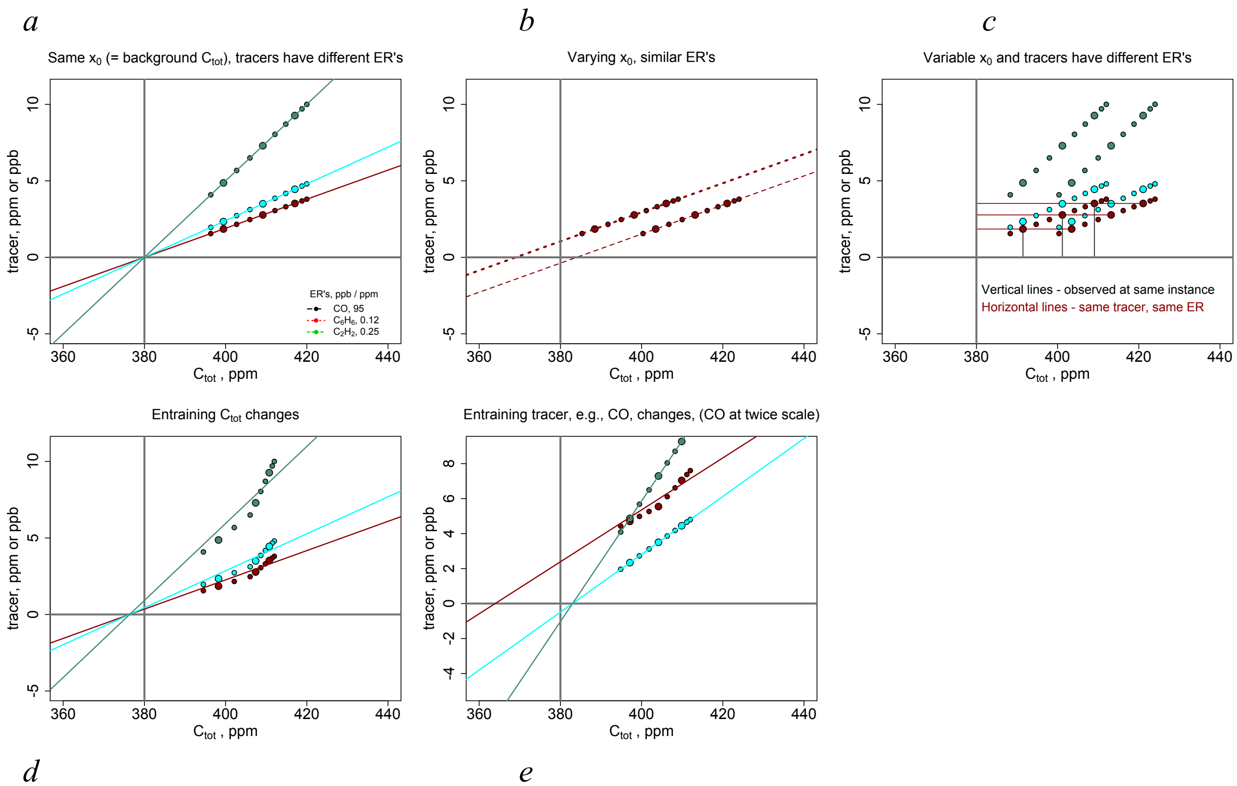

Figure 6. (a) Simulated dilution of three different fire tracers, EnRs as shown, and with environmental $\boldsymbol{x}^{\mathbf{E}}$of 380 ppm. These are nominally CO, benzene, and ethylene. Background concentrations of the tracers have been subtracted. C_{burn} is measured from the y-axis, where C_{tot} has the value 380 ppm. Larger dots highlight equivalent degrees of dilution. **(b)** Simulated dilution of one tracer, nominally CO above background, with different background $\boldsymbol{x}^{\mathbf{E}}$. Backgrounds are illustrated by the *x* intercepts. **(c)** Simulation of three tracers, varying EnRs and varying backgrounds (deducible from the x intercepts). Thin lines emphasize similar constant y values with different backgrounds, and constant $\boldsymbol{x}^{\mathbf{0}}$ values with varying EnRs. **(d)** Simulations like (a), but with a change of the $\boldsymbol{x}^{\mathbf{E}}$ entrained $\boldsymbol{x}^{\mathbf{0}}$ = C_{burn} background from 395 ppm to 375 ppm at the time of the 8th dilution step. A single applicable background value ~378 ppm is a linear interpolation between 395 and 375 ppm. **(e)** Simulation where background xE remains constant, but background CO changes by 1.5 ppb during the time (CO drawn at twice height for visibility).

This formula is the basis for the NEMR technique mentioned above, with *j* = CO playing a particularly important role. The inequality restrictions should be evaluated for an EnR to be a candidate for an ER and then an EF. In some cases, the background values, x^{Ea}, y_j^{Ea}, might be estimated from measurements made outside the plume. It can be somewhat more difficult to estimate x^{Eb}, y_j^{Eb} upwind of the source, especially for for air entraining into the fire plume at its source. A plume may also entrain air from various backgrounds and at various times during lofting and spread. That is, the history of entrainment may well be more complex than two conditions, "*a*" and "*b*", and the number of situations where we may estimate EnRs and then EFs is greatly limited. This important realization was described by Yokelson et al. (2013). The NEMR method can deal with most differences in x^{Eb} but not $y_j^{Eb}$for most tracers, and the quantity y_{CO}^{Eb} for carbon monoxide must be well sampled and well understood.

4.2. Examples showing robustness of computations of idealized C_{tot}

We used this approach to produce the following concrete examples of increasing complexity. They illustrate the origin of the features seen in Fig. 6 in terms of this simple plume dilution model. They helped motivate our solution techniques and indicate methods of analysis of individual plumes. These examples indicate possible limitations, but they also indicate a comforting averaging behavior of the linear differential equations as they describe our solutions. These uniformities and deviations also showed up in the analyses that we develop below. The examples also give some quantitative feel on the effects of deviations from the simplest hypothesis, e.g., x^{E} and y_j^{E} remain constant through time Fig. 6 shows calculations describing behaviors of x and the y_j in several plausible situations. Each graph represents the development of plume mixing ratios for a period of plume doubling, similar to the analysis time chosen in Poppe et al. (1998), following their equations Eq. 7 and Eq. 8. The dots show equal increments of plume expansion. Most parameters defining the equations may be read from the graphs themselves. Each initial concentration is shown by the points to the upper right of the line, i.e., the points with maximum $x = C_{\mathrm{burn}}$ and y_j = tracer concentration for each case considered.

Figure 6 (a) illustrates a plume history for x^{E} = 380 ppm and EnRs with respect to airborne C_{tot} of 95 x 10^{-3} ppm/ppm, 12 x 10^{-6} ppm/ppm, and 25 x 10^{-6} ppm/ppm, which are reasonable values for carbon monoxide (in ppb), benzene, and ethylene (in ppt). In the figures, focus attention on the relative behavior of the tracers. It is assumed that there are no consequential production or destruction reactions and also that there is a constant background tracer concentration, which has been subtracted. The individual plots show situations of increasing complexity. Fig. 6a shows the dilution behavior of the three species. A constant dilution rate is plotted; note that varying dilution rate changes the spacing of the dots but not the linear pattern. Larger dots highlight equivalent dilution of tracer and $x = C_{\mathrm{tot}}$ as would be observed in hypothesized discrete airplane samples. Figure 6b illustrates the dilution of CO in environments with differing entrained x^E. In Fig. 6a the larger dots align vertically, in Fig. 6b, horizontally. Figure 6c illustrates the situation where both EnRs and backgrounds vary; the thin lines emphasize independent aspects of EnR and x^E. The points on the x axis where (excess) tracer is zero are important to our estimation technique, more important than x^E. Estimation of x^E utilizes data on the vertical lines, while EnRs utilize information from both the vertical and horizontal lines. Statistically speaking, the problem of estimation of both backgrounds and EnRs illustrates simultaneous effects that are "separable". The reader may wish to extend the analysis to a large sequence of changes in entrained concentrations and note the essential linearity of this aspect of the formulation and that the solution expresses an appropriate averaging effect. We remark that the near uniqueness of the solutions obtained below (making small allowances for measurement error) will underline the robustness of the solutions.

However, the effect of uniform variations in background tracer concentrations y_j^{E} is not completely solved in this work. y_j^{E} can be estimated by examining the lowest values y_j^{E} in non-plume air; it is best to exclude values that appear to have contributions of exotic air (e.g., stratospheric air) or possible measurement problems at very low mixing ratios (e.g. negative values). Restricting attention to larger values of x_i and y_{ij} greatly ameliorates problems arising from y_j^{E} .

5. Theory: A regression relationship for EnRs

Let us consider more broadly the equations that provide a basis for statistical estimation. For current purposes of explanation, we make the seemingly large assumption that points from different plumes have similar properties at the same degree of dilution and may be compared. That is, the a_j are consistent for all plumes. Effects of varying x^E and y_j^E between the plumes may be largely taken out by regression; that is our current concern. Later, we will describe our approach to address possible variations in the EnR relationships a_j for parcels in the same or different plumes.

The basis of MERET utilizes the concept of the unmeasured extreme where $y_{aj} = 0$. To begin with, we consider the situation where (i) the emissions relationships a_j are constant for all observations and (ii) background values of the tracers are small enough in a relative sense, i.e., $|y_j^{Ea} - y_j^{Eb}| \ll |y_{aj} - y_{bj}|$. That condition is common for many species that have loss timescales of less than a month and/or have small non-fire sources. Each of these restrictions can eventually be relaxed. In this case

$$y_a = a_j\,(x_a - \{x_b - x^{Eb} + x^{Ea}\}) + \{y_j^{Ea} - y_j^{Eb}\} \qquad (13a)$$

\

$$y_a = a_j\,(x_a - \{x_b - x^{Eb} + x^{Ea}\})\,,\ \text{for } |y_j^{Ea} - y_j^{Eb}| \ll |y_{aj} - y_{bj}| \qquad (13b)$$

notice that terms within braces can be estimated by regression as sums, varying by the situation b. What if the values of these terms change discretely in time, for example as a plume leaves a daytime mixed layer, or distinct upper-air plumes are encountered? Simple algebra with linear formulas suggests that estimates of the terms in braces change discretely. Gradual changes of entrained mixing ratios of course imply a continuity condition on these terms.

We return to the illustrative dilution behaviors described in Fig. 6. Figure 6(d) describes a sudden change of background x^E by 20 ppm, x^{Eb} to x^{Ea}, midway in the expansion/dilution; at this stage of plume evolution, 20 ppm is about four times larger than typical fire contributions to C_{tot}. Estimates of x_i^0 from a few samples along these lines (without knowledge of the time of change) would be intermediate. Equations 13 suggests that the EnR estimate need not be affected. Some similar calculations make it clear that the estimates average satisfactorily under varied assumptions. Figure 6(e) shows a very contrasting behavior, when there is a sudden change in concentration of entraining tracer (CO) during plume dilution, a change of 1.5 ppm. In comparison, the addition of CO by burning at the start of the interval is ~3.5 ppm. We may distinguish this as $\hat{x}_{ij}^0$, where the j = CO and the hat indicates an estimate. This graph also suggests that if there are more than three tracers (we use 8), then the median of all the estimates, median ($\hat{x}_{ij}^0$), is robust against errors resulting if a tracer j has a variable or poorly described background resulting in $\hat{x}_{ij}^0$ at falling distinctly higher or lower than the others. We must be concerned about this since tracers can have occasionally important non-fire sources. Change in background of a tracer compared to observed change due to fire is critical in determining its usefulness in determining a useful estimate of the background x^0 as the well as the quality of its EnR of a tracer. Methane in particular has long atmospheric lifetime and several sources of similar strength; in California, livestock and fossil-fuel extraction significantly influence mixed-layer concentrations flowing into a fire updraft. Consequently, it can exhibit variations that are more than 10% of the fire emission contribution for well dispersed plumes.

The preceding discussion suggests that we may use the specialized least-squares technique,

(14)

$$y_{ij} = a_j(x_i - x_i^0) + e_{ij}$$

where x_i^0 expresses several terms of Eq 13, and any other corrections not proportional to a_j. We may call x_i^0 an "effective background." However, it is not a specific background, but actually summarizes the whole effect of changes in C_{bkgd} and also the degree of dilution. This means that the regression can synthesize information from not just one well-characterized plume but also different plumes provided we expected them to have similar a_j behavior. Figure 7 illustrates the use of regression employing the ideas developed in Fig. 6. Using the same formulas as above, we depict observations made of CO, C_6H_6, and C_2H_2 made at three instances (times). The three tracers determine a value x^0, and given that information, the three tracer enhancements and therefor tracer EnRs are determinable. The nested gray triangles, similar triangles, illustrate this idea for each of two values of $\boldsymbol{x^0}$ corresponding to two observation instances when it is assumed that $\boldsymbol{x^0}$ has changed. MERET uses the idea that the slopes must be equal. This simulation assumes no error in the measurements of CO_2+CO or the tracers, and assumes no variation in the EnRs, so values are determined perfectly.

How well are these situations with multiple observation instances and multiple tracers determined? In the case of two samples and two tracers, i.e., $N_{Instance} = 2$ samples and $N_{Tracer} = 2$ slopes (EnRs), we need to estimate x_1, x_2, a_1, a_2, and x_0 using only y_{11}, y_{12}, y_{21}, and y_{22}, there are not enough measured variables to determine a unique solution, $N_{Tracer} + N_{Instance} + 1 > N_{Tracer} \bullet N_{Instance}$, *viz.*, 5 > 4 . However, if there are three tracers, $N_{Tracer} \bullet N_{Instance} > N_{Tracer} + N_{Instance} + 1$, and we get a solution. Any measurement error, or indeed lack of perfect similarity in response slopes, can give somewhat conflicting solutions.

Figure 7 illustrates the use of regression employing the ideas developed in Fig. 6. Using the same formulas as above, we depict observations made of CO, C_6H_6, and C_2H_2 made at three instances (times). The three tracers determine a value x^0, and given that information, the three tracer enhancements and therefor tracer EnRs are determinable. The nested gray triangles, similar triangles, illustrate this idea for each of two values of $\boldsymbol{x^0}$ corresponding to two observation instances when it is assumed that $\boldsymbol{x^0}$ has changed. MERET uses the idea that the slopes must be equal. This simulation assumes no error in the measurements of CO_2+CO or the tracers, and assumes no variation in the EnRs, so values are determined perfectly.

How well are these situations with multiple observation instances and multiple tracers determined? In the case of two samples and two tracers, i.e., $N_{Instance} = 2$ samples and $N_{Tracer} = 2$ slopes (EnRs), we need to estimate x_1, x_2, a_1, a_2, and x_0 using only y_{11}, y_{12}, y_{21}, and y_{22}, there are not enough measured variables to determine a unique solution, $N_{Tracer} + N_{Instance} + 1 > N_{Tracer} \bullet N_{Instance}$, *viz.*, 5 > 4 . However, if there are three tracers, $N_{Tracer} \bullet N_{Instance} > N_{Tracer} + N_{Instance} + 1$, and we get a solution. Any measurement error, or indeed lack of perfect similarity in response slopes, can give somewhat conflicting solutions.

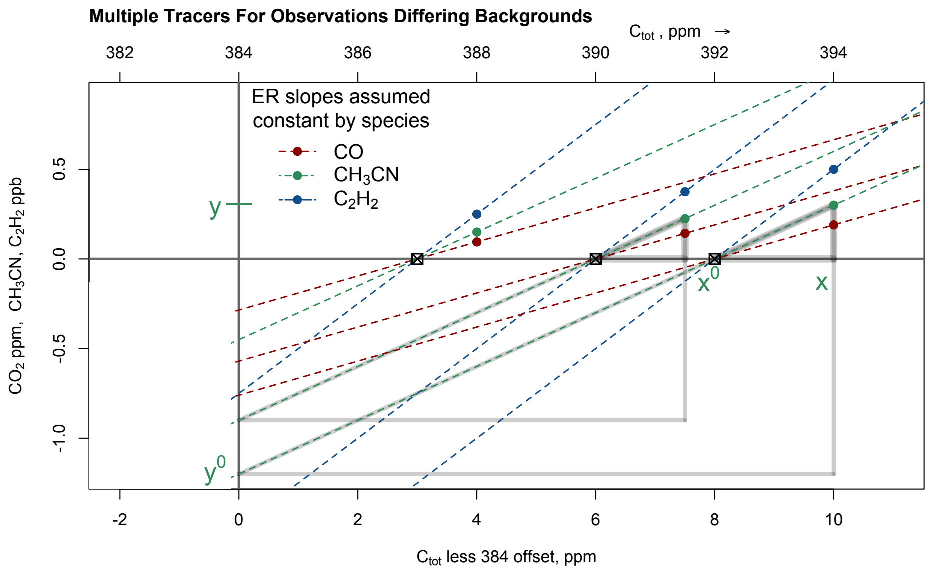

Figure 7. Multiple tracers allow solution for an equivalent background $\boldsymbol{x^0}$, illustrated by an idealized example largely replicating the conditions of fire plume sampling above an Amazonian mixed layer as described by Yokelson et al. (2013). The colored dashed lines indicate the theoretical response of tracer to the C_{tot} when C_{bkgd} takes on various values indicated by black squares. There are several lines shown the ideas expressed in Fig. 6a. The fact that the various colored lines associated with each x meet at the value with x-coordinate $\boldsymbol{x^0}$and y coordinate 0 represents the estimation that precisely solves equation (5) above. If we had included error in observations or variation in EnRs, there would be variations in the positions of $\boldsymbol{x^0}$ and the slopes. As the next section describes, regression of tracer *vs* C_{tot} is required and gives a spread of y-intercepts. Nevertheless, these can be mapped back to x-intercepts using slopes and the concept of similar triangles. The nested gray triangles illustrate this idea for each of two values of $\boldsymbol{x^0}$.

6. Methodology:

6.1. Finding the CO_2 + CO background

The use of tracers with backgrounds removed and then scaled to a common mean establishes a well-conditioned matrix problem and easier analysis of sensitivity effects. We have identified forest fire plume samples and N_{tracer} tracers whose background values can be reasonably estimated. Let us proceed with the regression and begin to address some complications that arise. The mathematical problem we must solve is Eq. 14, which we will rewrite to emphasize that we are starting in native units.

$$y_{ij}^{\mathrm{measured}} - y_j^{\mathrm{E}} = a_j(x_i - x_i^0) + e_{ij} \tag{15}$$

In the following development in this section, we will work with y_{ij} above background, i.e., set $y_{ij}^{\mathrm{pre-normalized}} \leftarrow (y_{ij}^{\mathrm{measured}} - y_j^{\mathrm{E}})$.

We must attempt to fit $y_{ij}^{\text{pre-normalized}}$ for each species *j* (1 to N_j) and for each measurement instance *i* (1 to N_j). The term e_{ij} describes the error. Besides removing backgrounds, we wish that each tracer *j* should contribute equally to the sum-of-squares that determine a regression, independent of its mean value. Consequently, we should normalize the tracers so that there mean is 1:

$$y_{ij} = y_{ij}^{\text{pre-normalized}} / \underset{i}{\text{mean}}\left(y_{ij}^{\text{pre-normalized}}\right)$$

We will use normalized values of the tracers for the following development until Equation 20. It is not necessary to normalize x_i, but it will be useful to subtract a baseline. This suggests that the basic regression equation might be the following

$$y_{ij} = a_j(x_i - x_i^0) + e_{ij} \tag{15}$$

Equation 15 also summarizes just why the determination of ERs is difficult: the equation is non-linear in the multiple regression sense: i.e., we must include the mixed *i*- and *j*-term $a_j x_i^0$ as a regression term. The problem is a mixed-effects model: we must estimate the statistics of two separately varying processes affecting x_i^0 and a_j.

A complication arises concerning the use of regression. The fire-tracer variables y_{ij} must "point back" to a zero-point, where no *C* was added by the burn, $C_{\text{burn}} \equiv x_i - x_i^0 = 0$, but that each instance *i* may have a different zero-point. A regression formula should solve this in some way. Commonly, regression fits provide a *y*-intercept, i.e., the value at *x* = 0. Here we have an *x*-intercept to estimate, i.e., the concentration of the reference species at zero added fire emissions, and so the problem becomes non-linear in the regression sense. In summary, we have a non-linear random effects model (Pinheiro and Bates, 2000), which requires specialized techniques.

One feature of Equation 15 is emphasized: the formulation does not require any relationship of the x_i or y_{ij} in time: instances must only represent a sufficiently coherent class of fires: one would expect more accuracy and discernment of features in similar forest fires, but not forest fires and grass fires. For the latter case, the assumption of consistent a_j becomes problematic.

Why not simply reverse the problem and seek *x* as a function of *y*?

$$x_i = \alpha_j \; y_{ij} - x_i^0 + e_{ij} \tag{16}$$

where the x_i^0 are estimated with a regression model (specifically a fixed-effects model). The difficulty is that the trivial solution $x_i = -x_i^0$ fits perfectly and was hard for us to avoid even when we attempted to restrict the solution with a non-linear solver. Is it not easier to convert y intercepts into x-intercepts? This appears more productive and should appeal to those not familiar with using a non-linear solver in this particular mode of non-linearity. In place of Equation 15, we may write a regression equation with an intercept:

$$\text{Regress} \quad y_{ij} = a_j x_i + c_i^0 + e_{ij} \tag{17}$$

where the *y*-intercepts, c_i^0, are estimated for each instance and the e_{ij} are minimized by least squares. The **R** expression used to solve this problem was

```
main.lmer = lmer( y ~ x + (x - 1 | species.type) + ( 1 | id ) + 1
```

where `id` indicates the sequential observation number for the tracer species. The term `species.type` indicates the species description *j*. The word `type` signals a generalization described in the next section. (This expression is written in a commonly used Wilkinson-Rogers (1973) symbolic form: The symbol ~ describes our intention to make a regression estimate. The vertical lines indicate how factors are involved with variables, 1 indicates an intercept is to be described by a random effect, and `(x - 1 | species.type)` indicates that a slope that multiplies *x* is to be estimated, indexed by `species.type`. "No intercept estimated" is signaled by –1.) The regression results generates a set of *fitted y* values which we may call $\hat{y}_{ij}$ and a set of *fitted* $\hat{a}_j$ values. Together, the values of x_i, $\hat{y}_{ij}$, and $\hat{a}_j$ imply a *y*-intercept y_{ij}^0 when $x_i = 0$ as shown in Fig. 7. One evaluates the fit for $x_i = 0$. Then one may use the slopes estimates $\hat{a}_j$ of a_j by regression to find the several estimates $\hat{x}_{ij}^0$ provided by

$$\hat{x}_{ij}^0 = (\hat{y}_{ij} - y_{ij}^0)/\hat{a}_j \tag{18}$$

This is where we use the similar triangles concept of Fig. 7. The use of a single $\hat{a}_j$ for all observation instances of the same species (more precisely, `species.type`) is a strong constraint on the resulting estimate. This is how for $\hat{a}_j$ and $\hat{x}_{ij}^0$ how we use the concept of the similar triangles described in Fig 7 of the last section.
We then take

$$\hat{x}_i^0 = \underset{j}{\text{median}}\ \hat{x}_{ij}^0 \tag{19}$$

The estimation of $\hat{x}_i^0$, now allows estimates of the incremental carbon liberated to the atmosphere, $C_{\text{burn}} = (x_i - \hat{x}_i^0)$. We will drop the hat from $\hat{x}_i^0$ below, writing x_i^0 and $C_{\text{burn}} = (x_i - x_i^0)$ except when we wish to emphasize their nature as estimates. Emission factors for individual tracer species may be obtained directly by adding fixed and random effects on slopes for each species and each observation, $\hat{a}_{\text{j}}$. An enhancement ratio for any concentration or property y_j with a background, measured at time *i* in the aircraft sampling can be obtained using the carbon-burned estimate

$$\text{EnR for } y_{ij} = \frac{\left(y_{ij}^{\text{measured}} - y_j^{\text{E}}\right)}{\left(x_i - x_i^0\right)} \equiv \left(y_{ij} - y_j^{\text{E}}\right)/(C_{\text{burn}})_i \tag{20}$$

To repeat, the variable y_{ij} now stands for any property for which we seek an EnR, for example ozone, which is not one of the eight indicator variables. y_j^{E} describes a non-fire-dependent background value. This ratio estimate is available for all tracers, and is preferred over a similar slope variable $\hat{a}_j$ used to estimate x_i^0 in the in equation 18 above.

Formulas for the statistics of ratio quantities with uncertainties in numerator and denominator can be theoretically complex, so we simply computed error estimates by simulation using computed Bernoulli trials. One thousand samples of normal distributions were calculated each for the numerator and the denominator, using their uncertainties as 1σ values. Then the ratios of the first numerator and first denominator normal deviate sample, the second, … to the 1000th normal deviate sample for numerator divided by the 1000th normal deviate sample were calculated, and the distribution of ratios summarized. For the numerator, the measured value and the suggested standard deviation (typically a percentage ratio) provided the parameters for the normal distribution. For the denominator, the mean was the C_{burn} estimate, and the standard deviation was a value of 0.25 ppm, documented as the measurement error (precision + bias) of CO_2. (See Table 1). Uncertainties in the calculation of $\hat{x}_i^0$ were considered small and did not add to the dispersion of the denominator, especially since it is clear that any additive biases contributing to the quoted uncertainty of (CO_2+CO) cancel out. Sample calculations in the supplementary material (SM: "Note on Sensitivity to number of tracers used"**).** suggest errors typically of magnitude 0.03 ppm due to variations in technique, and usually <0.1 ppm. Additive errors should also cancel out for the numerator, since a background is subtracted. Indeed, some tracers like ethene appeared to have a negative background as determined from plots and simple regression calculations of y_{ij} on $(C_{\text{burn}})_i$. This is not unexpected, since these compounds are sampled into cans, where a small but self-limiting coating of the measured species on the can surfaces might cause such a negative offset, and yet the integrity of the can sample at larger values might be little affected.

6.2. Practicalities: variable EnRs

Equations 17–19 provide the basis of the MERET technique. There are however some details that increase its relevance and accuracy. First there is normalization. Common practice is to normalize all the tracer species *j* with respect to the mean of all observations of species *j*, after subtracting a baseline. This allows each tracer to influence y_{ij} equally. Assigning weights accomplishes the same purpose, but scaling allows better diagnostic graphs. In fact, the literature referenced above emphasizes how informative *j* = CO is, despite its relatively small variation in EnR or slope. Consequently, we give CO twice the weight of all the other species.

Secondly, we allow for a certain amount of true variation in the EnRs, expecting this to make equation 18 perform better. This is done by imagining that virtual species can be associated with "fire types" for example "flaming CO" or "smoldering CO" or "high-nitrogen-fuel CH_3CN". A "fire-type" is a value for each observation that applies to all tracer species at that instance. It expresses commonalities between different mixes of burning emissions, commonalities that may be more frequently or less frequently expressed in any given plume, e.g., "smoldering-CO fire-type". We might speculate on the nature of the fire-type, e.g. "smoldering" or "derived from nitrogen-rich fuel". However, we let the statistical technique define these types, and so apply basic clustering techniques. We used non-negative matrix factorization (NMF), but Mahalanobis clustering or other techniques seem to do as well. NMF is more fully described in a companion paper describing patterns linking EnRs for several compounds; NMF and *k-means* clustering are shown to be equivalent in cases corresponding to our work (Ding et al., 2005). A larger number of cluster classes will allow more ability to follow the EnR actually characteristic of the observation, but at the cost of parsimony and sensitivity to instrumental error for the species or property. We used the **R** routine *nmf()* with *k* = 6 components and the Lee estimation technique with singular value initialization (Lee and Seung, 2001, et al, 2001, Boutsidis and Gallopoulos, 2008). Use of the singular-value option for initialization proved satisfactory; it agreed well with the default method.

Since all fire tracers are correlated, such clustering characterizations are much better defined if based on a rough normalization to the fuel burned. We used a consensus variable, composed from all the defining tracers, to act as an agent for constructing ratios,

$$\nu_i = \underset{j}{\mathrm{mean}}\left(y_{ij}\right) \tag{21}$$

This ratioing variable plays a role logically played by $C_{\mathrm{burn}} = (x_i - x_i^0)$. Exact quantitative calibration of C_{burn} in ppm is not required, just a relative scale. We found it could be intuitively helpful to conceive of the ratioing variable in ppm of carbon, just as our later estimate of C_{burn}. To assign ppm values, see SM: "Note on an Early Approximate C_{burn}".

We end this section on methodology describing a separate strand of analysis. We sought timescales that could be inferred from the data, which could distinguish the relative age of burning emissions. At greater distances from the fire, there is both aerosol transformation and photochemical loss/production of species. Photochemical processing appeared easier to diagnose. We followed the ideas of Roberts et al. (1984), McKeen and Liu (1984), Parrish et al. (2007), and Warneke et al. (2013). The Parrish et al. presentation was most directly relevant. For considerations of these plume samples, a single origin strongly controlling mixing ratios made analysis simpler. Following Parrish's Equation 3, and using the symbols E and Y are the mixing ratios of ethEne, and ethYne, respectively,

$$\tau_{\text{age}}(\text{OH}) = -\frac{1}{k_E - k_Y}\left(ln\frac{y_Y}{y_E} - ln\frac{ER_{\text{Y}}}{ER_{\text{E}}}\right) \tag{22}$$

In view of this we constructed estimates for each instance i of $\log_{10}((y_Y)_i/(y_E)_i)$ – Constant. The Constant can be estimated with similar results (a) so that the shortest times are about +15 minutes, or (b) from the highest observed values of $\log_{10}((y_Y)_i/(y_E)_i)$. The values of longer times are determined by the assumed value of [OH]. The references cited describe the fact that most $\tau_{\text{age}}(\text{OH})$ observations have a contribution from mixing as well as photochemistry, but this has little effect on the relative ages. In view of the uncertainty of the history of [OH] during transport, we simply graph the log of the ratios. Data analysis suggested that the assumed back-ground mixing ratios of the species of ethyne and ethene were small. The supplementary material provides some more details and one estimate of the associated times. SM: "Note on Sensitivity to number of tracers used"

6.3. Summary of the MERET algorithm and notes

A summary of the MERET method as we currently propose it is shown in Fig. 8. It contains many steps, due to the need to disentangle background $(C_{\text{burn}})_i$ effects from a_j effects related to instance-by-instance EnRs and the variation of $\hat{a}_j$ by fire-type.

1. Select a dataset of likeliest forest-fire emission plumes, CH_3CN > 0.125 ppt (clear biomass-burning signal) and excluding urban influence $(CO–CO^{Env})/(CO_2– CO_2^{Backg}) > 33 \times 10^{-3}$.

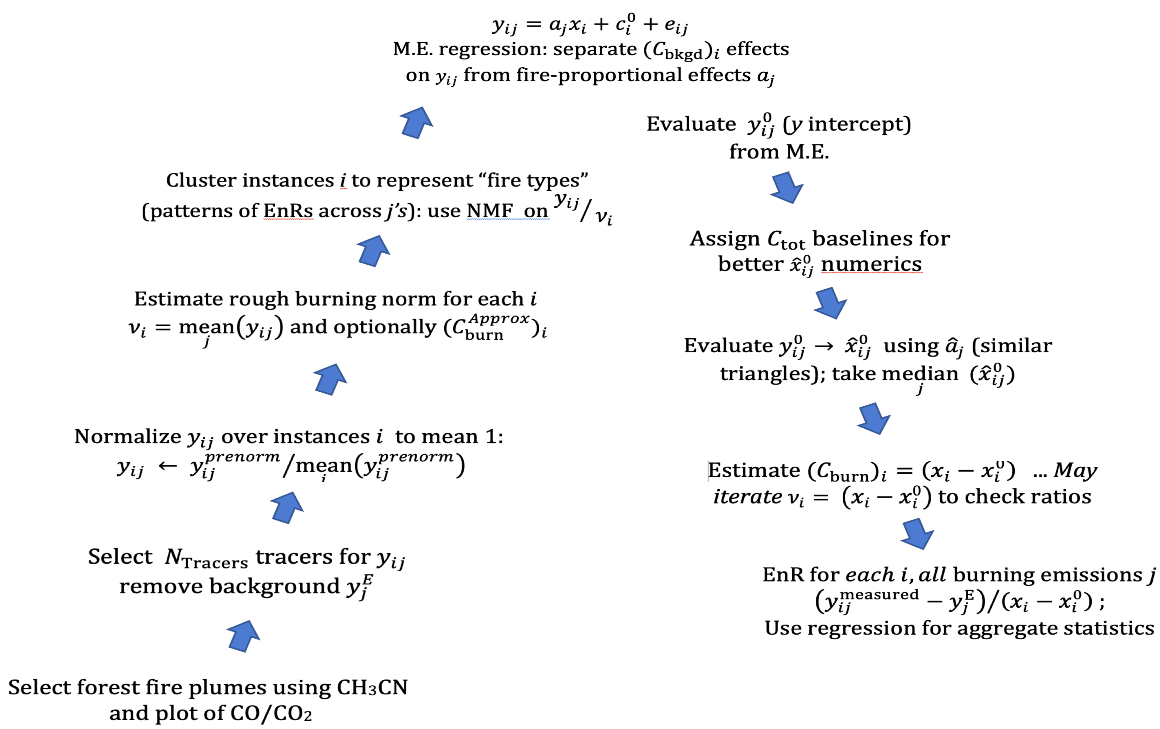

Figure 9. Summary of the MERET algorithm. See text for further detail.

2. Select $N_{\text{Tracer}} > 3$ fire tracers with estimable environmental background values y_j^E and subtract from plume instances. Nearby values sufficiently distant from plumes provide a good guide unless tracer has very strong non-fire sources (e.g. CH_4 in California valleys). $y_{ij}^{\text{pre-normalized}} \leftarrow (y_{ij}^{\text{measured}} - y_j^{\text{E}})$.
3. *Normalize* the tracers above backgrounds: $y_{ij} = y_{ij}^{\text{pre-normalized}} / \underset{i}{\text{mean}}\left(y_{ij}^{\text{pre-normalized}}\right)$
4. Create values *ratioed* to a general fire-influence parameter: $\nu_i = \underset{j}{\text{mean}}\left(y_{ij}\right)$, Create y_{ij} / ν_i. May estimate preliminary $\left(C_{\text{burn}}^{\text{Approx}}\right)_i$ based on ν_i, for reference.
5. Roughly cluster plumes into N_{Types} clusters using ratioed values y_{ij} / ν_i to estimate fire types corresponding to varying EnRs common to species *j*. The value of N_{Types} was observed to make little difference. We used $N_{\text{Types}} = 6$. Allow *j* to signify tracers within clusters.
6. Use mixed effects regression to make estimates of intercepts and slopes $\hat{y}_{ij}^0$ and $\hat{a}_j$ using a mixed effects regression like `main.lmer`, allowing random effects corresponding to species (or species and type of fire) and by instance Regress $y_{ij} = a_j x_i + c_i^0 + e_{ij}$ and estimate the fitted values $\hat{y}_{ij}$
7. Prepare to estimate $\hat{x}_{ij}^0$. For numerical reasons, select an offset to apply to plumes that follows lower plume values, approximately 2 ppm less. Better discrimination makes for tighter estimates of $\hat{x}_{ij}^0$ in next step.
8. Calculate $\hat{x}_{ij}^0 = (\hat{y}_{ij} - y_{ij}^0) / \hat{a}_j$ from the fitted $\hat{y}_{ij}$ values: take $\hat{x}_i^0 = \underset{j}{\text{median}}\ \hat{x}_{ij}^0$ Medians are little affected by exact choices in 7, but spread of estimate are affected.
9. Estimate $\left(C_{\text{burn}}\right)_i = \left(x_i - \hat{x}_i^0\right)$. The results for equivalent background $\hat{x}_i^0$ and C_{burn} are shown in Fig. 9, and are discussed more in Section 7. EnRs may now be calculated using equation 20. One may also use $(C_{\text{burn}})_i$ recursively, returning to steps 4–9 until convergence. However, for our dataset this made inconsequential difference.
10. Use $\left(x_i - \hat{x}_{ij}^0\right)$ to estimates EnRs for any fire emission including tracers, using EnR for each i and $j = \left(y_{ij}^{\text{measured}} - y_j^{\text{E}}\right) / (x_i - x_i^0)$; evaluate EnR to estimate ER and EF, considering possible transformation from emission to measurement point.

More technical observations are these:

(a) Use of an offset in calculations: We subtracted a baseline, C_{baseline},, a value determined as a constant for contiguous intervals, shown later in Section 7, Fig. 9, and yielding a ~2 ppm offset. We found that this minimized *skewness* and *variance* in the $\hat{x}_{ij}^0$ estimates for each observation instance *i*. It is comforting that the effect of differing offsets on the values of the *median*, x_i^0 is small, < 1 ppm. (Add the offset back in the C_{baseline} when reporting x_i^0).

(b) Note that sharp positive and negative excursions of x_i^0 are seen near dramatic spikes in x_i. However, $(x_i - x_i^0)$ and consequently the EnRs are little affected. We can only speculate that small differences in the time averaging of CO_2 and the tracers due to the instruments may explain these. Note also that the number of parameters $N_{\text{Tracer}} \cdot N_{\text{Types}} + N_{\text{Instance}}$ for the mixed effects regression remains << $N_{\text{Tracer}} \cdot N_{\text{Instance}}$ so that the mixed effects regression is very strongly determined.

(c) The number of classes allowed in step 5 matters little over 2 or 3. Adding additional classes (clusters) tends to add only minor variations in the slopes $\hat{a}_j$. We are aware that overfitting effects can occur with many regression terms with positive and negative terms which mainly allow fitting of special cases. Here, harmful effects seen in over-fitting of regression models are largely avoided by a requirement that the $\hat{a}_j$'s be positive.

(d) As noted, it is possible to use this method recursively, making presumably better classifications of fire types. In our experience, while it is possible to make convergent, recursive characterizations of the C_{burn} quantity, tighter clustering, and more precise mixed-model *lmer()* estimates, the quantities x_i^0 and $(x_i - x_i^0)$ were just significant to warrant such care. If we had available fewer than 8 tracers, such recursion might be important. We will incrementally update documentation of the code (Chatfield, 2020). New applications of the code will suggest improvements.

A Check on the consistency of C_{burn} estimation: The results for C_{burn} and tracer EnRs suggested to us that one likely source of uncertainty is that C_{burn}, $\hat{x}_i^0$, and the tracers may change very rapidly in comparison to our one-minute sampling intervals. Looking into this, we found that many of the C_{burn} estimates are of small magnitude, 12 of the 422 samples yielded $C_{\mathrm{burn}} <$ 1.5 ppm. Even large jumps from sample to sample in estimated $\hat{x}_i^0$ were not particularly associated with anomalous estimates of C_{burn}. The remaining, appealing possibility is occasional imprecise time alignment of all measurements, particularly of the CO_2 measurements. Such imprecise alignment could happen at any stage, from sampling line delays to interpolation to one-minute time intervals. Such variations in CO_2 would affect the $\hat{x}_{ij}^0$ found for all tracers in a coordinated way, just as was observed. Note that estimates of C_{burn} were little affected, since significant $\hat{x}_{ij}^0$ excursions were associated with large CO_2+CO values. See SM: "Note on Examples of Enhancement Ratios."

6.4. Number of independent samples

A natural broader question is: "How well do these mean EnRs for a species represent the EnRs that might be measured in a large suite of significant forest fires in the Western US?" Clearly, this question can only be asked in the context of the sample provided by the two campaigns. Instances when the aircraft continued to sample smoke for many minutes could contain several types of plumes, as we will see illustrated for the Rim Fire Plume of August 2013. The use of 10-sec averages (if available) would not provide six times as much information about fire plumes as 60-sec averages over the same measurement run. We tried a simple, approximate quantification of "independent instances" available to us using a frequently used formulation by Trenberth 1984). This can also be seen as providing one answer to the question "How many effectively independent samples of C_{burn} are there contributing to a mean, standard deviation, etc., of C_{burn}, … or of CO tracer?" That could be useful if instruments appeared to give imprecise measurements that required averaging. Trenberth assessed the correlation of successive observations by estimating an autoregressive AR(1) (i.e., Markov chain) model for a random variable ξ_i with parameter ϕ and random error ε_i, i.e., estimate of $\xi_{i+1} = \phi\, \xi_i + \varepsilon_i$. We applied this for $\xi_i = x_i - x^0$ ($= C_{\mathrm{burn}}$) and several fire tracers y_{ij}, like toluene. Most contiguous sampling periods suggested around 0.6; this suggested Trenberth's "effective time between independent observations" as $\approx (1+\phi)/(1-\phi)$, about 4 minutes. Four minutes corresponds to about 15 km at lower-tropospheric airspeeds for the DC-8. The effect of this on the formal standard errors as described by a normal distribution was to increase them by a factor of ~2. Roughly similar effects are expected for the empirical descriptions of EnR variability described below. Undoubtedly, for plumes within minutes of the source, the number of degrees of freedom corresponds more closely to the number of 1-min observations, but the number of such samples is low.

Not surprisingly, *residuals* in regressions of CO against C_{burn} are very little correlated. We surmise that such low correlation gives confidence in the mathematical determination of the mean regression slope. However, it does not provide help in answering the larger question, that of relevance in new situations. The sequential samples of plumes may have features like non-stationarity and selection bias; we hope that these ideas suggest more sophisticated analyses of relevance, left to future work.

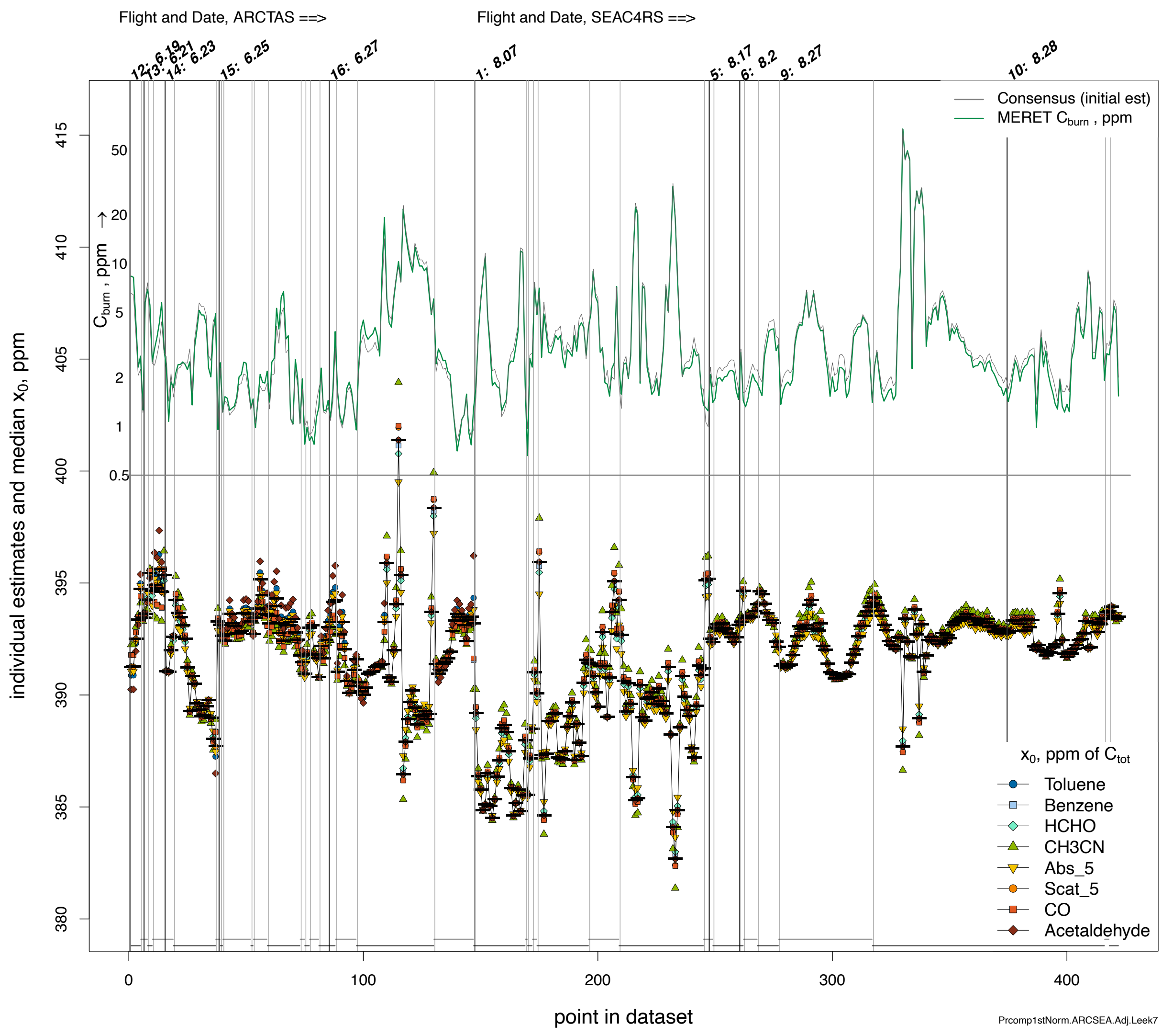

Figure 9. (Lower panel). Estimates of the 422 background $\hat{x}_i^0$ = CO_2+CO concentrations implied based on the 8 fire tracers indicated in the legend. Contributing individual estimates $\hat{x}_{ij}^0$ are shown by overlapping colored points, with the median estimate $\hat{x}_i^0$ indicated by a black bar. Usually the colored points overlap closely, this indicates strong agreement **(Upper panel)** Estimates of $\boldsymbol{C}_{\mathrm{burn}} = \boldsymbol{x}_i - \hat{\boldsymbol{x}}_i^0$ indicators of fuel carbon burned, in the heavy green line. The preliminary estimate of $\boldsymbol{C}_{\mathrm{burn}}$ based on the consensus of tracer deviations (without variable EnR estimates) is also shown in a light line. A scale factor, maximizing overlap

with the heavy line, was necessarily estimated by regression. Flight days are indicated by the days marked on the top axes, and individual plumes, separated by non-plume concentrations of longer than 10 minutes, are shown as vertical separator lines. A set of horizontal lines at ~400 ppm indicates selected intervals for optimizing numerics (see text, Section 6.3, item 7).

7. Results: Estimation of x_i^0 and C_{burn}

The important results of the mixed model are the background $\hat{x}_i^0$, and even more importantly the incremental carbon liberated to the atmosphere, $C_{\text{burn}} = x_i - \hat{x}_i^0$. The background estimates of $\hat{x}_i^0$ for all samples and the contributing individual estimates $\hat{x}_{ij}^0$ are shown in FIG.9. The median $\hat{x}_i^0$ is shown as a thin black line. The colored circles in the legend identify how the tracer species j contribute an individual $\hat{x}_{ij}^0$. determining the median $\hat{x}_{ij}^0$.

What are the uncertainties in the estimates of $\hat{x}_i^0$ and C_{burn} we have made? The uncertainty in estimated carbon burned $(x_i - \hat{x}_i^0)$ plays an important role in the ultimate estimates, the emission factors. In this section, we will confine our exposition to this uncertainty for now. The graphs of $\hat{x}_i^0$ and $(x_i - \hat{x}_i^0)$ shown in Fig. 9 provide a practical understanding of the uncertainty. Note the continuity in $\hat{x}_i^0$; this important observation is described below.Traditional estimation of uncertainties for $(x_i - \hat{x}_i^0)$ is complex due to the several steps involved and the use of median estimates. The advisability of using the median estimator and its statistical properties have long been recognized (Laplace, 1774; Lawrence, 2013). This variety of uncertainty estimation may be useful as the MERET technique is refined. However, we expect that the study of uncertainty depends more on evaluating sources of true variability in the EnRs and also on the conservation of tracer concentrations from the flames to the sampling point than on the mathematics of median estimation. Consequently, the following paragraphs explore these questions related to the number and choice of tracers. We suggest that the typical strong overlap of the individual-tracer values may high precision of the observer's techniques!

How does the number of tracers affect results? What are the effects of using alternate or simpler sets of tracers? How many tracers are required for stable estimates? We began to address these questions by examining estimates made with fewer tracers in the intercept-determining set: the selection of the set of j's. The supplementary material gives two examples of subsets. (SM: "Note on Sensitivity to Number of Tracers Used") Here is a summary of that material. The two sets chosen are those that are the most unambiguous indicators of $\hat{x}_{ij}^0$ based on their mutual agreement with $\hat{x}_i^0$ from the full set of 10 tracers. They are Set 1 (CO, Scat_5, and HCHO) and Set 2 (CO, Scat_5, HCHO, acetaldehyde, and toluene). These are indicated by a examination of Fig. S8 in the Supplementary Material. (Abs_5 contributed $\hat{x}_{ij}^0$ most varying from $\hat{x}_{ij}^0$.) Set 2 gave variations around 0.02 ppm, the smaller set, Set 1, gave very similar variation except for the flights of June 22 and 25, where many observation instances varied by around 0.1 ppm, but with 11 points out of 422 differing by 0.3 ppm. This level of agreement surprised us. More significantly to our aims, the relative error in C_{burn} was only about 2%. When sets containing the less correlated tracers were used, deviations ranged up to 0.2–0.4 ppm, which appeared still remarkably small.

Observation-to-observation consistency in $\hat{x}_i^0$-estimates, seen for most plumes observed in Fig. 9, is the strongest argument for the precision of the C_{burn} estimates. Recall, our theory does not use sequential time information: thus, successive estimates are essentially independent of each other. There is of course the dependency due to each observation's contribution to the estimate as one component of the *entire dataset*. This continuity is maintained even though the magnitudes of CO_2+CO and estimated C_{burn} can change dramatically as the sampling aircraft enters and leaves each plume. Smooth excursions seen early in the flight marked 8.27 are explicable in terms of large changes in sampling altitude and location around the Rim Fire on that day. There are variations in $\hat{x}_i^0$ from plume to plume and day to day.

In contrast to this typical continuity of $\hat{x}_i^0$-estimates, there are 15 to 20 brief and large excursions which deserve some attention. Of course, these may be disregarded in getting a general picture of EnRs. All the tracers suggest these excursions of the median, although there is a larger variation between the individual tracer-based estimates $\hat{x}_{ij}^0$. These excursions are always associated with large changes in CO_2+CO and C_{burn}, but often they occur one minute later. We examined these excursions in detail. They do not seem to relate to changes in the EnRs $\hat{a}_j$ (as qualified by fire-type) estimated simultaneously. The observations y_{ij} and the fitted $\hat{y}_{ij}$ agree well, as well as for non-excursion points. Note however, that we may only use a single set of fire types, independent of j, to construct set of $\hat{a}_j$'s and $\hat{y}_{ij}$ to make the $\hat{x}_{ij}^0$ estimates.

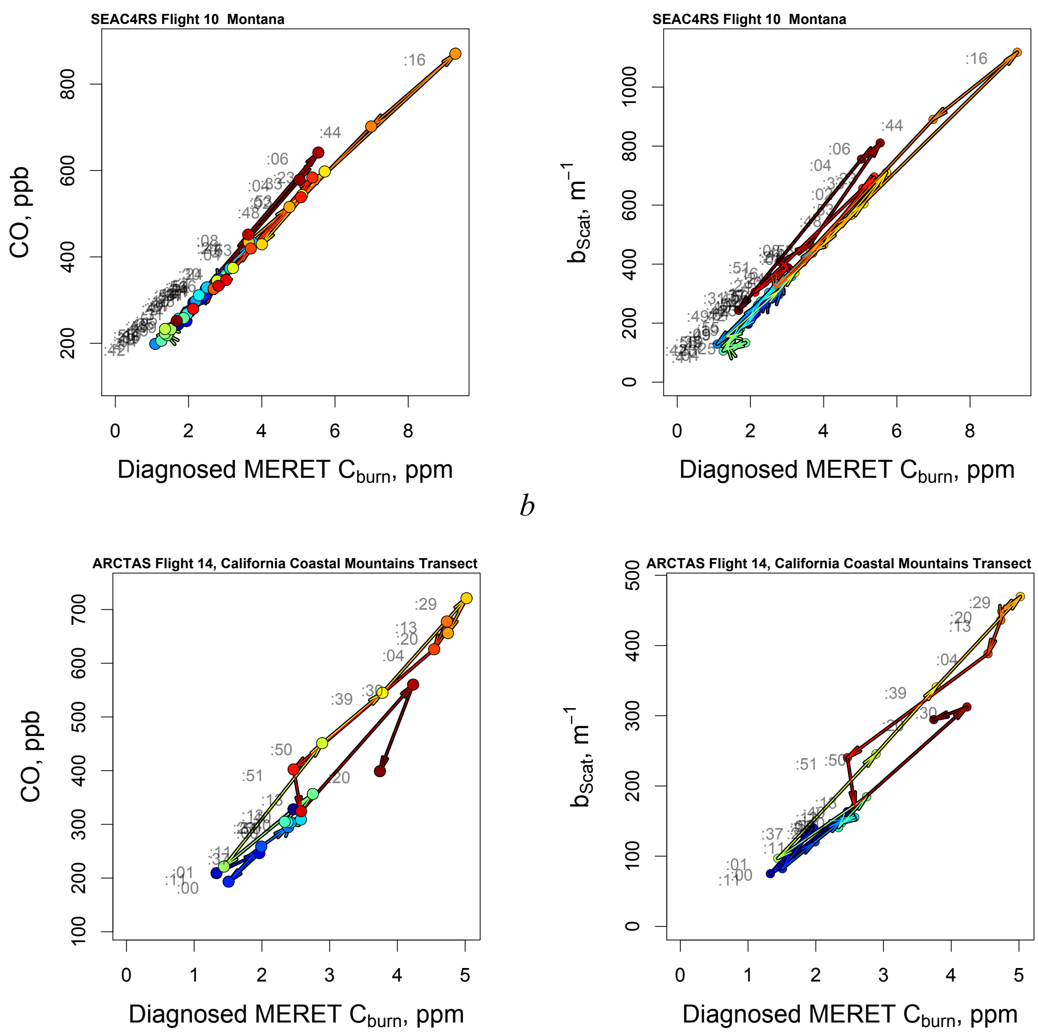

a *b*

c *d*

Figure10. Analyzed relation of tracers to carbon burned using the MERET technique for portions of SEAC4RS Flight 10 and ARCTAS Flight 14. Compare **(a)** through **(d)** with Fig. 4, b, c, e, and f. Colors key the observations to times shown in the timelines, Fig. 4a and Fig. 4(c). Light gray numerals give observation times in minutes.

The results for C_{burn} and tracer EnRs suggested to us that one likely source of uncertainty is that C_{burn}, $\hat{x}_i^0$, and the tracers may change very rapidly in comparison to our one-minute sampling intervals. This would seem to be a concern since some C_{burn} estimates are of small magnitude: 12 of the 422 samples yielded $C_{\mathrm{burn}} < 1.5$ ppm. However, large jumps from sample to sample in estimated $\hat{x}_i^0$ were not particularly associated with anomalous estimates of C_{burn}. The remaining, appealing possibility is occasional imprecise time alignment of all measurements, particularly of the CO_2 measurements. Such imprecise alignment could happen at any stage, from sampling line delays to interpolation to one-minute time intervals. Such variations in CO_2 would affect the $\hat{x}_{ij}^0$ found for all tracers in a coordinated way, just as was observed. Note that estimates of C_{burn} were little affected, since significant $\hat{x}_{ij}^0$ excursions were associated with large CO_2+CO values.

MERET should work better with more tracers, since more fire-types may be revealed. However, additional classes (clusters) tend to add only minor variations in the slopes $\hat{a}_j$. Furthermore, harmful effects often seen in over-fitting of regression models should be minimized by a requirement that the $\hat{a}_j$'s be positive. (Positive and negative regression coefficients cannot be added that allow fitting of just a few points.)

8. Estimates of emissions ratios: Two MERET examples

8.1. MERET results for our two examples

The usefulness of our estimates of $\hat{x}_i^0$ and $C_{\mathrm{burn}} = x_i - \hat{x}_i^0$ is seen in the MERET analysis (Fig. 10) of the two case studies analyzed above using the NEMR approach, where portions of Flights 10 and 14 were shown in Fig. 4. The tracers CO and b_{scat} appear much better correlated with the C_{burn} estimated from MERET, especially in Flight 14. The plots for both CO and scattering imply linear relationships with an implied intercept near 0, i.e., background values of y_i have been satisfactorily removed. Difficulties with a variable C_{bkgd} appear to be resolved. However, the slopes of all the lines do not all agree. The Montana scatterplots (a) and (b) appear to suggest two slightly different linear features. The California Transect scatterplots (c) and (d) show more separated linear features, though the slopes are parallel. We expect that these might correspond to varying fire types, perhaps varying MCE's, to be discussed in Chatfield and Andreae (2020), or to variations in background values y_j^0, which are much harder to detect with either MERET or NEMR. A combined approach, using MERET to locate regions of similar MCE, might be useful here. Also, note that the variation of slope is more evident for b_{scat} than CO emphasizing the special role of CO as a single best fire tracer, closely followed by b_{scat}.

8.2. Table of several significant emissions

Table 3 provides a summary of the EnR relationships for some of the most significant gaseous emissions and particulate properties. In many cases, these EnRs can be converted to ERs and emission factors when the relationship of airborne C_{burn} to surface fuel consumed can be established. For the most highly reactive species, these EnRs will tend to be underestimates. An interpretive paper (Chatfield and Andreae, 2020) will give additional information on the photochemical age of the observation in many cases. Ozone and peroxy acetyl nitrate (PAN) are not emissions, but produced in the plumes. The relationships to fuel burned, and their variations are nevertheless interesting. Descriptions of variation are given as the 16th and 84th percentiles of all the estimates. These are similar to error estimates if nothing more is known about the origin and age of the particular samples, a matter more fully discussed in Chatfield and Andreae (2020). EnR's as they varied in time, and in relationship to measures of photochemical processing, are shown in the SM: "Note on Examples of Enhancement Ratios Variation in Time."

Table 3. EnR Estimates for Fire Emissions Considered

Fire Emission	EnR estimate	Percentile 16	Percentile 84	Unit	Conversion factor to EF
CO	74	62	85	ppb ppm^{-1}	1.17
CH_4	8.6	2.3	13.0	ppb ppm^{-1}	0.67
Ethyne	0.26	0.205	0.31	ppb ppm^{-1}	1.08
Ethene	0.88	0.65	1.07	ppb ppm^{-1}	1.17
Ethane	0.70	0.57	0.80	ppb ppm^{-1}	1.25
Propene	0.056	0.005	0.100	ppb ppm^{-1}	1.75
Propane	0.16	0.12	0.19	ppb ppm^{-1}	1.83
n-Butane	0.028	0.019	0.037	ppb ppm^{-1}	2.17
Benzene	0.094	0.073	0.134	ppb ppm^{-1}	3.25
Toluene	0.054	0.023	0.067	ppb ppm^{-1}	3.88
Methanol	2.1	1.7	3.1	ppb ppm^{-1}	1.33
HCHO	1.15	0.81	1.62	ppb ppm^{-1}	*1.25*
Acetaldehyde	0.56	0.24	0.71	ppb ppm^{-1}	1.83
Acetone	0.74	0.54	1.14	ppb ppm^{-1}	2.42
CH_3CN	0.13	0.11	0.16	ppb ppm^{-1}	1.25
NO_x (as N)	0.051	0.024	0.131	ppb ppm^{-1}	0.63
O_3	14.8	8.5	25.1	ppb ppm^{-1}	*(2.0)*
PAN	0.26	0.17	0.38	ppb ppm^{-1}	*(3.17)*
Scat_5, b_{Scat}	79	50	100	m^{-1} ppm^{-1}	0.042
Abs_5, b_{Abs}	3.2	2.2	4.4	m^{-1} ppm^{-1}	0.042
Ammonium	0.32	0.19	0.47	µg m^{-3} ppm^{-1}	0.032
Nitrate	0.28	0.11	0.60	µg m^{-3} ppm^{-1}	0.107
Sulfate	0.156	0.063	0.290	µg m^{-3} ppm^{-1}	0.164

Notes: Conversions assume a C to dry biomass ratio of 0.5. Conversions to µg m^{-3} assume 25 ºC and 1013 hPa. O_3 and PAN are not directly produced by fires. HCHO is produced but often decreases rapidly. Under appropriate conditions indicated in Chatfield and Andreae (2020), the EnR estimates can be used as ERs. For tracers that are rapidly removed or transformed, these tend to be the higher values.

9. Conclusions

A major problem with the estimation of fire enhancement ratios and emission factors is inherent in their character: flames promote mixing in their plumes. Total carbon liberated to the atmosphere (approximately $C_{\mathrm{burn}} = CO_2+CO$) is mixed with background air at different points in the plume's evolution, and removal of that mixing effect has been a difficulty. The NEMR technique often uses CO as unique tracer, but the EnR of CO is variable, adding uncertainty to the estimation of the EFs. Given the variability of CO due to combustion efficiency (MCE) and environmental variability, it has been emphasized that the NEMR technique can only be confidently applied in situations in which conditions affecting the ratio of CO to (CO_2+CO) can be well determined, ideally from source to sampling (Yokelson et al., 2013). The method also tends to emphasize the use of samples of CO and tracer collected over many minutes, so that the regression method for EnRs of tracer relative to CO, defining, $a_{\mathrm{CO} \leftarrow (\text{fire-added } C_{\mathrm{burn}})}$ becomes stable, and a conversion to fuel carbon burned becomes possible.

We sought to decompose C_{tot} into C_{bkgd} and C_{burn}. However, meteorology and mixing allow significant variations in C_{bkgd} due to other powerful processes, e.g., CO_2 from respiration/photosynthesis in mixed-layer air. Once lofted, C_{bkgd} varies little unless the plume enters layers of free tropospheric air from long-range transport with different C_{bkgd}, which further dilute the plume (Yokelson et al., 2013). We noted such problems using NEMR in analyzing a significant number of plumes for enhancement ratios studied in the Western US during two campaigns, ARCTAS-California and SEAC4RS, with 422 one-minute samples in all.

The problem of deriving an accurate C_{bkgd} is solved by noticing that there are two different kinds of information provided by multiple observational instances of a tracer and multiple tracers at a single instance. Information about the various EnRs and C_{bkgd} are mixed, but not inextricably. There is a solution based on mixed-effects (also called random effects) regression modeling. We propose a Mixed Effects Regression Emissions Technique (MERET) to replace or at least to check on NEMR, for which we used the **R** routine *lmer()*.

The MERET technique is related to traditional entraining-plume models for parcels. We presented a synthesis describing multiple tracers from fire to sampling location. Sample calculations with the model suggest that it deals linearly several varied histories for plume mixing. This motivates a regression equation for an "equivalent background" x_i^0 for each observation that is related to entraining concentrations $x^E(t)$ along the trajectory, and shows coherent agreement for each tracer species (Fig. 9). The theory then allows this x_i^0 to be used to define C_{burn} and thus to define the EnR for any appropriate fire-derived variable. This technique should allow EnRs in more variable, difficult situations, and allows estimates of EnRs for individual samples.

EnRs are useful for the estimation of emission factors when the plume age is short compared to the transformation timescale of the measured fire tracer, and we provide an approximate diagnostic for this age for most samples. Formaldehyde, acetaldehyde, the alkenes, benzene, NO_x, b_{Scat}, and b_{Abs} particularly require such attention.

Carbon monoxide is usually the best single tracer that correlates with fire emissions (C_{burn}), supporting the use of the NEMR technique. Our analysis suggests other tracers had EnR variations that collectively helped to distinguish C_{burn} from CO in regression. The NEMR methodology depends on a full analysis of the history of CO influences on a sample to obtain a reliable MCE. MERET allows estimates of MCE as well as C_{burn} for each sample. Thus it demarcates sampling periods with nearly homogeneous MCE. However, possible large variations in the entraining background of CO should still be considered carefully in dilute plumes with C_{burn} <2 ppm.

9.1. Questions for future research

We conclude with some questions for future research; these also review the suggested conclusions of this paper and acknowledge the limitations of a single publication.

(1) How well can the use of one or a few tracers, e.g., CO, b_{scat}, HCHO, actually constrain EnRs and EFs when only a few instruments may be used? How many variables need to be measured or how fresh should the plumes be to allow CO to be used both as a fire tracer and to allow useful estimates of MCE?

(2) Can MERET be used to identify time periods of relatively homogeneous MCE, and can that MCE value be used with NEMR to create suitable EnRs? Since NEMR uses differences sample by sample (in time), no minimum value of another tracer need be estimated. (Consider that MERET does allow some evaluation of the minimum value estimate to be assessed and a better minimum assigned.)

(3) Can the MERET/NEMR and better near-fire non-plume sampling help us to prevent misattribution of fire emissions? These would include observations for fire intake air, air likely to be entrained in ascent, and air surrounding a plume and likely to be entrained as a plume spreads downwind. Can simulations of entraining plumes aid this effort?

(4) What do "fire types" represent and which species or properties tend to correlate in their EnRs (Chatfield and Andreae, 2020).

Science Team List

ARCTAS Science Team:

James Crawford (NASA Langley Research Center), Henry Fuelberg (Florida State University), Chris Hostetler (NASA Langley Research Center), Daniel Jacob (Harvard University), Hal Maring (NASA Headquarters), Philip B. Russell (NASA Ames Research Center), Kent Shiffer (NASA Ames Research Center), Hanwant Singh (NASA Ames Research Center), Kathy Thompson (Science Systems and Applications, Inc.), Bruce E. Anderson (NASA Langley Research Center), Eric Apel (National Center for Atmospheric Research), Donald R. Blake (University of California Irvine), William H. Brune (Pennsyvania State University), Christopher A. Cantrell (National Center for Atmospheric Research), Ronald C. Cohen (University of California Berkeley), Jack Dibb (University of New Hampshire), Glenn S. Diskin (NASA Langley Research Center), Alan Fried (University of Colorado), Johnathan W. Hair (NASA Langley Research Center), L. Greg Huey (Georgia Tech), Jose-Luis Jimenez (CIRES, University of Colorado), Yutaka Kondo (University of Tokyo), Richard E. Shetter (University of North Dakota), Robert Talbot (University of New Hampshire), Stephanie A. Vay (NASA Langley Research Center), Rodney Weber (Georgia Tech), Andrew Weinheimer (National Center for Atmospheric Research), Paul Wennberg (Cal Tech), Armin Wisthaler (Universitãt Innsbruck and Universitatet i Oslo), John Barrick (NASA Langley Research Center), Anthony Bucholtz (Naval Research Laboratory), Antony Clarke (University of Hawaii), Lawrence C. Freudinger (NASA Armstrong Flight Center), Charles Gatebe (NASA Goddard Space Flight Center), Athanasios Nenes (Georgia Tech), James Podolske (NASA Ames Research Center), Jens Redemann (University of Oklahoma), Sebastian Schmidt (CU Boulder), Anthony Strawa (NASA Ames Research Center), Brian Cairns (NASA Goddard Institute for Space Science), Richard Ferrare (NASA Langley Research Center), Samuel Oltmans (NOAA ESRL, CU Boulder), Glenn Shaw (University of Alaska Fairbanks), Anne

M. Thompson (NASA Goddard Space Flight Center), Bob Curry (NASA Armstrong Flight Center), David Easmunt (NASA Goddard Space Flight Center), Michael S. Wusk (NASA Langley Research Center).

SEAC4RS Science Team:
Hal Maring (NASA Headquarters), Ken Jucks (NASA Headquarters), Jassim Al-Saadi (NASA Headquarters), Richard Eckman (NASA Headquarters), Alex Pszenny (NASA Headquarters), Kent Shiffer (NASA Ames Research Center), Jhony Zavaleta (NASA Ames Research Center), Michael Craig (NASA Ames Research Center), David Jordan (NASA Ames Research Center), Quincy Allison (NASA Ames Research Center), Dan Chirica (NASA Ames Research Center), Susan Tolley (NASA Ames Research Center), Erin Czech (NASA Ames Research Center), Erin Justice (NASA Ames Research Center), Katja Drdla (NASA Ames Research Center), Brian Toon (University of Colorado), Eric Jensen (NASA Ames Research Center), Rich Ferrare (NASA Langley Research Center), David Diner (NASA Jet Propulsion Laboratory), Anthony Bucholtz (Naval Research Laboratory), Lance Christensen (NASA Jet Propulsion Laboratory), Matt McGill (NASA Goddard Space Flight Center), Steve Platnick (NASA Goddard Space Flight Center), Brian Cairns (NASA Goddard Space Flight Center), Jim Anderson (Harvard University), Rushan Gao (NOAA ESRL), Bob Herman (NASA Jet Propulsion Laboratory), MJ Mahoney (NASA Jet Propulsion Laboratory), Rushan Gao (NOAA ESRL), Steve Wofsy (Harvard University), Sebastian Schmidt (University of Colorado), Elliot Atlas (University of Miami), Paul Bui (NASA Ames Research Center), Hanwant Singh (NASA Ames Research Center), Jack Dibb (University of New Hampshire), Phillip Russell (NASA Ames Research Center), Jose-Luis Jimenez (University of Colorado), Charles Brock (NOAA ESRL), Simone Tanelli (NASA Jet Propulsion Laboratory), Andreas Beyersdorf (NASA Langley Research Center), Anthony Bucholtz (Naval Research Laboratory), Samual Hall (National Center for Atmospheric Research), Paul Wennberg (Cai Tech), Thomas Ryerson (NOAA ESRL), Glenn Diskin (NASA Langley Research Center), Armin Sorooshian (University of Arizona), Alan Fried (National Center for Atmospheric Research), John Hair (NASA Langley Research Center), Glenn Diskin (NASA Langley Research Center), Greg Huey (Georgia Tech), Rushan Gao (NOAA ESRL), Thomas Hanisco (NASA Goddard Space Flight Center), Bruce Anderson (NASA Langley Research Center), Paul Bui (NASA Ames Research Center), Karl Froyd (NOAA ESRL), Greg Huey (Georgia Tech), Armin Wisthaler (Universität Innsbruck), Jack Dibb (University of New Hampshire), Paul Lawson (SPEC Incorporated), Sebastian Schmidt (University of Colorado), Ronald Cohen (University of California Berkeley), Donald Blake (University of California Irvine), Joshua Schwarz (NOAA ESRL), J. Vanderlei Martins (University of Maryland Baltimore County), Lenny Pfister (NASA Ames Research Center), Henry Fuelberg (NASA Langley Research Center), Rennie Selkirk (Universities Space Research Association), Daniel Jacob (Harvard University), Arlindo Da Silva (NASA Goddard Space Flight Center), Paul Konopka (Georgia Tech), Ed Hyer (Naval Research Laboratory), Greg Charmichael (University of Iowa), Jennifer Olson (NASA Langley Research Center), Louisa Emmons (National Center for Atmospheric Research), Gao Chen (NASA Langley Research Center), Chip Trepte (NASA Langley Research Center), Jay Mace (University of Utah), Pat Minnis (NASA Langley Research Center), Eric Ray (NOAA ESRL), Karen Rosenlof (NOAA ESRL), Daniel Jacob (Harvard University), Robert Yokelson (University of Montana), Jeffery Reid (Naval Research Laboratory), Jens Redemann (NASA Ames Research Center), David Starr (NASA Goddard Space Flight Center), Johnny Luo (City College of New York), Jay Mace (University of Utah), Laura Pan (National Center for Atmospheric Research),

David Starr (NASA Goddard Space Flight Center), Jay Mace (University of Utah), Johnny Luo (City College of New York), James Crawford (NASA Langley Research Center), Frank Culter (NASA Armstrong Flight Center), Patrick Lloyd (NASA Armstrong Flight Center), Rick Shetter (National Suborbital Education and Research Center), Adam Webster (National Suborbital Education and Research Center), Eric Buzay (National Suborbital Education and Research Center), David VanGilst (National Suborbital Education and Research Center), Jane Peterson (National Suborbital Education and Research Center), Tim Moes (NASA Armstrong Flight Center), Chris Miller (NASA Armstrong Flight Center), Mike Kapitzke (NASA Armstrong Flight Center), Denis Steele (NASA Armstrong Flight Center), Stuart Broce (NASA Armstrong Flight Center), Jan Nystrom (NASA Armstrong Flight Center), Kevin Kraft (NASA Armstrong Flight Center).

Some of the team have changed affiliations since their work was documented. Two members of NASA's Earth Science Projects Office (ESPO) may direct you on how to make enquiries regarding either team, marilyn.vasques@nasa.gov and bernadette.luna@nasa.gov. Also, a leader at NASA Headquarters, has some knowledge of both teams' members, barry.lefer@nasa.gov.

Data availability: ARCTAS and SEAC4RS data are available for download from these permanent NASA data repositories: Arctic Research of the Composition of the Troposphere from Aircraft and Satellites (ARCTAS, https://www-air.larc.nasa.gov/missions/arctas/arctas.html, and SEAC4RS – Studies of Emissions and Atmospheric Composition, Clouds and Climate Coupling by Regional Surveys https://www-air.larc.nasa.gov/missions/seac4rs/.

Supplement: The supplement related to this article is available on- line at: (TBD)

Acknowledgements Particular acknowledgment goes to the instrumental groups in Table 1 and Section 4 and the many contributing efforts of the ARCTAS and SEAC4RS Science Teams and staff. The effort grew out of research funded by California Air Resources Board and San Joaquin Valley air regional authority, where difficulties with previous methodology became apparent. We appreciate reviews by S. Palacios, M. Segal-Rozenhaimer, E. Yates, and especially R. Koppmann.. Robert F. Esswein helped with certain data reformatting. We acknowledge the great value of the **R** programming language and the lme4 and NMF packages.

Author contributions MOA contributed motivating ideas and approach following on Yokelson et al. (2013). RBC brought data into suitable format and evaluated suitability of tracers. He contributed the theory of parallel plume rise expressions for fire tracers and the mixed-effects modeling approach. RBC wrote the publication with considerable contributions of MOA.

Competing Interests: The authors declare that they have no competing interests.

Financial support. This research has been partially supported by the US NASA Earth Sciences Research program research grant 13-ACCDAM13-0110, ACMAP14-0095, and Earth Sciences salary support in association with more recent fire studies. M. O. Andreae acknowledges extensive support by the German Max Planck Society and facilitation of recent research by the Scripps Institute of Oceanography

10. References

Akagi, S. K., Yokelson, R. J., Burling, I. R., Meinardi, S., Simpson, I. J., Blake, D. R., McMeeking, G. R., Sullivan, A., Lee, T., Kreidenweis, S., Urbanski, S., Reardon, J., Griffith, D. W. T., Johnson, T. J. and Weise, D. R.: Measurements of reactive trace gases and variable O_3 formation rates in some South Carolina biomass burning plumes, Atmospheric Chemistry and Physics, 13, 1141–1165, doi:10.5194/acpd-12-25255-2012, 2013.

Akagi, S. K., Yokelson, R. J., Wiedinmyer, C., Alvarado, M. J., Reid, J. S., Karl, T., Crounse, J. D. and Wennberg, P. O.: Emission factors for open and domestic biomass burning for use in atmospheric models, Atmospheric Chemistry and Physics, 11, 4039–4072, doi:10.5194/acpd-10-27523-2010, 2011.

Akagi, SK, et al. Evolution of trace gases and particles emitted by a chaparral fire in California, Atmos. Chem Phys., 12, 1397-1421, 2012.

Alvarado, M. J. and Prinn, R. G.: Formation of ozone and growth of aerosols in young smoke plumes from biomass burning: 1. Lagrangian parcel studies, J. Geophys. Res.-Atmos., 114, doi:10.1029/2008jd011144, 2009.

Alvarado, M. J., Wang, C. and Prinn, R. G.: Formation of ozone and growth of aerosols in young smoke plumes from biomass burning: 2. Three-dimensional Eulerian studies, J. Geophys. Res.-Atmos., 114, doi:10.1029/2008jd011186, 2009.

Alvarado, M. J., Logan, J. A., Mao, J., Apel, E., Riemer, D., Blake, D., Cohen, R. C., Min, K. E., Perring, A. E., Browne, E. C., Wooldridge, P. J., Diskin, G. S., Sachse, G. W., Fuelberg, H., Sessions, W. R., Harrigan, D. L., Huey, G., Liao, J., Case-Hanks, A., Jimenez, J. L., Cubison, M. J., Vay, S. A., Weinheimer, A. J., Knapp, D. J., Montzka, D. D., Flocke, F. M., Pollack, I. B., Wennberg, P. O., Kurten, A., Crounse, J., St Clair, J. M., Wisthaler, A., Mikoviny, T., Yantosca, R. M., Carouge, C. C. and Le Sager, P.: Nitrogen oxides and PAN in plumes from boreal fires during ARCTAS-B and their impact on ozone: an integrated analysis of aircraft and satellite observations, Atmos. Chem. Phys., 10(20), 9739–9760, doi:10.5194/acp-10-9739-2010, 2010.

Andreae, M. O.: Emission of trace gases and aerosols from biomass burning – An updated assessment: Atmos. Chem. Phys. Discuss., 2019, 1-27, doi:10.5194/acp-2019-303, 2019.

Andreae, M. O. and Merlet, P.: Emission of trace gases and aerosols from biomass burning, Global Biogeochemical Cycles, 15(4), 955–966, doi:10.1029/2000GB001382, 2001.

Andreae, M. O., Browell, E. V., Garstang, M., Gregory, G. L., Harriss, R. C., Hill, G. F., Jacob, D. J., Pereira, M. C., Sachse, G. W.,Setzer, A. W., Silva Dias, P. L., Talbot, R. W., Torres, A. L., and Wofsy, S. C.: Biomass burning emissions and associated haze layers over Amazonia, J. Geophys. Res., 93, 1509–1527, 1988.

Barry, R.G., Chorley, R.J.: Atmosphere, Weather and Climate (7th edition), Routledge (London), 1998.

Bates D, Maechler M, Bolker B and Walker S: lme4: Linear mixed-effects models using Eigen and S4. R package version 1.1-7, http://CRAN.R-project.org/package=lme4, http://arxiv.org/abs/1406.5823, 2014.

Baylon, P., Jaffe, D. A., Wigder, N. L., Gao, H. and Hee, J.: Ozone enhancement in western US wildfire plumes at the Mt. Bachelor Observatory: The role of NO_x, Atmospheric Environment, 109, 297–304, doi:10.1016/j.atmosenv.2014.09.013, 2015.

Boutsidis, C., and Gallopoulos, E.: SVD based initialization: A head start for nonnegative matrix factorization, In: Pattern Recognition 41., 1350–1362. issn: 00313203. doi: 10.1016/j.patcog.2007.09.010, 2008.

Burling, I. R., Yokelson, R. J., Griffith, D. W. T., Johnson, T. J., Veres, P., Roberts, J. M., Warneke, C., Urbanski, S. P., Reardon, J., Weise, D. R., Hao, W. M. and de Gouw, J.: Laboratory measurements of trace gas emissions from biomass burning of fuel types from the southeastern and southwestern United States, Atmospheric Chemistry and Physics, 10(22), 11115–11130, doi:10.5194/acp-10-11115-2010, 2010.

Chatfield, R.B.: package Estim.ARC.SEAC.ERs, https://github.com/RobertBChatfield/FireEmissionsEstimate/, 2002.

Chatfield, R.B., and Andreae, M.O.: Emissions relationships among western forest fire plumes: II. Plume typing for sources of ozone and aerosol absorption, advanced draft in preparation for Atmos. Chem. Phys. 2020.

Crutzen, P.J., Heidt, L.E., Krasnec, J.P., Pollock, W.H., Seiler, W., Biomass burning as a source of atmospheric gases CO, H_2, N_2O, NO, CH_3Cl and COS. Nature 282, 253e256, 1979. P J. Crutzen, L E. Heidt, J P. Krasnec, W H. Pollock and W Seiler: Biomass burning as a source of atmospheric gases CO, H_2, N_2O, NO, CH_3Cl, and COS, Nature, 282, 253–256, 1979.

Crutzen, P.J., and Andreae, M.O.: Biomass Burning in the Tropics: Impact on Atmospheric Chemistry and Biogeochemical Cycles, Science, 250, no. 4988, 1669–1678, DOI:10.1126/science.250.4988.1669, 1990.

DeCarlo, P. F., Kimmel, J. R., Trimborn, A., Northway, Megan J., Jayne, J. T., Aiken, A. C., Gonin, M., Fuhrer, K., Horvath II, T., Docherty, K. S., Worsnop, and D. R., Jimenez, J.L.: Field-Deployable, High-Resolution, Time-of-Flight Aerosol Mass Spectrometer, Anal. Chem. 78, 8281-8289, 2006.

Ding, C., He, X., and Simon, H.D.: On the Equivalence of Nonnegative Matrix Factorization and Spectral Clustering, Proceedings of the 2005 SIAM International Conference on Data Mining, 10.1137/1.9781611972757.70, also permalink https://doi.org/10.1137/1.9781611972757.70, 2005.

Forrister, H., Liu, J., Scheuer, E., Dibb, J., Ziemba, L., Thornhill, K. L., Anderson, B., Diskin, G., Perring, A. E., Schwarz, J. P., Campuzano-Jost, P., Day, D. A., Palm, B. B., Jimenez, J. L., Nenes, A., and Weber, R. J.: Evolution of brown carbon in wildfire plumes, Geophys. Res. Lett., 42, 4623–4630, https://doi.org/10.1002/2015GL063897, 2015.

Frenklach, M., Reaction mechanism of soot formation in flames: Physical Chemistry Chemical Physics, 4, 2028-2037, doi:10.1039/b110045a, 2002.

Fried, A., Walega, J. G., Olson, J. R., Crawford, J. H., Chen, G., Weibring, P., Richter, D., Roller, C., Tittel, F. K., Heikes, B. G., Snow, J. A., Shen, H., O'Sullivan, D. W., Porter, M., Fuelberg, H., Halland, J., and Millet, D.: Formaldehyde Over North America and the North Atlantic During the Summer 2004 INTEX Campaign: Methods, Observed Distributions, and Measurement-Model Comparisons, J. Geophys. Res.,{113, }D10302, https://doi.org/10.1029/2007JD009185, 2008.

Galanter, M., Levy II, H., and Carmichael, G. R.: Impacts of biomass burning on tropospheric CO, NO_x, and O_3, J. Geophys. Res., 105, 6633–6653, doi:10.1029/1999JD901113, 2000.

Gaujoux, R., Seoighe, C.: A flexible R package for nonnegative matrix factorization, BMC Bioinformatics 11.1 p. 367. issn: 1471-2105. doi: 10.1186/1471-2105-11-367, 2010.

Gaujoux, R.:An Introduction to NMF package, https://cran.r-project.org/web/packages/NMF/vignettes/NMF-vignette.pdf, 2014.

Greenberg J. P., Zimmerman P. R., Heidt L., and Pollock W.: Hydrocarbon and carbon monoxide emissions from biomass burning in Brazil, J. Geophys. Res. 89 (D1), 1350–1354. 1984.

Gueniche, H. A., Biet, J., Glaude, P. A., Fournet, R., and Battin-Lederc, F.: A comparative study of the formation of aromatics in rich methane flames doped by unsaturated compounds: Fuel, 88, 1388-1393, doi:10.1016/j.fuel.2009.03.006, 2009.

Guyon, P., Frank, G. P., Welling, M., Chand, D., Artaxo, P., Rizzo, L., Nishioka, G., Kolle, O., Fritsch, H., Silva Dias, M. A. F., Gatti, L. V., Cordova, A. M., and Andreae, M. O.: Airborne measurements of trace gases and aerosol particle emissions from biomass burning in Amazonia: Atmos. Chem. Phys., 5, 2989–3002, 2005.

Hanna, S.R, Briggs, G.A., Hosker, R.P.: Handbook on Atmospheric Dispersion. Prepared for the US Department of Energy, Technical Information Center, US Department of Energy(DOE/TIC-11223), 1982.

Hobbs, P. V., Sinha, P., Yokelson, R. J., Christian, T. J., Blake, D. R., Gao, S., Kirchstetter, T. W., Novakov, T., and Pilewskie, P.: Evolution of gases and particles from a savanna fire in South Africa, J. Geophys. Res., 108, 8485, doi:10.1029/2002JD002352, 2003.

Hornbrook, R. S., Blake, D. R., Diskin, G. S., Fried, A., Fuelberg, H. E., Meinardi, S., Mikoviny, T., Richter, D., Sachse, G. W., Vay, S. A., Walega, J., Weibring, P., Weinheimer, A. J., Wiedinmyer, C., Wisthaler, A., Hills, A., Riemer, D. D., and Apel, E. C.: Observations of non-methane organic compounds during ARCTAS − Part 1: Biomass burning emissions and plume enhancements, Atmos. Chem. Phys., 11, 11103-11130, https://doi.org/10.5194/acp-11-11103-2011, 2011.

Jaffe, D., Wigder, N.: Ozone production from wildfires: a critical review. Atmos. Environ. 51, 1–10, http://dx.doi.org/10.1016/j.atmosenv.2011.11.063, 2012.

Janhäll, S., Andreae, M. O., and Pöschl, U.: Biomass burning aerosol emissions from vegetation fires: particle number and mass emission factors and size distributions, Atmos. Chem. Phys., 2001, 10, 1427-1439, doi:10.5194/acp-10-1427-2010.

Koppmann, R., A. Khedim, J. Rudolph, D. Poppe, M. O. Andreae, G. Helas, M. Welling, and T. Zenker: Emissions of organic trace gases from savanna fires in southern Africa during the 1992 Southern African Fire Atmosphere Research Initiative and their impact on the formation of tropospheric ozone, J. Geophys. Res., 102, 18,879– 18,888, 1997.

Koppmann, R., von Czapiewski, K., and Reid, J. S.: A review of biomass burning emissions, part I: gaseous emissions of carbon monoxide, methane, volatile organic compounds, and nitrogen containing compounds, Atmos. Chem. Phys.., 5, 10455-10516, https://doi.org/10.5194/acpd-5-10455-2005, 2005

Langridge, J. M., Richardson, M. S., Lack, D. A., Law, D. C., and Murphy, D. M.: Aircraft instrument for comprehensive characterization of aerosol optical properties, Part I: Wavelength-dependent optical extinction and its relative humidity dependence measured using cavity ring-down spectroscopy, Aerosol Science and Technology, 45, 1305-1318 doi10.1080/02786826.2011.592745, 2011.

Laplace, P.S., Mémoire sur la Probabilité des Causes par les Évènemens, Mémoires de Mathematique et de Physique, Presentés à l'Académie Royale des Sciences, Par Divers Savans & Lûs Dans ses Assemblées, 6, 621-656, 1774.

Lawrence, J.: Distribution of the Median in Samples from the Laplace Distribution, Open Journal of Statistics, 3 (6), DOI:10.4236/ojs.2013.36050, 2013.

Lee, D.D., and Seung. H.S.: Algorithms for non-negative matrix factorization, Advances in Neural Information Processing Systems, url: http://scholar.google.com/scholar?q=intitle:Algorithms+for+non-negative+matrix+factorization, 2001.

Leeuwen, T. T., and G. R. van der Werf: Spatial and temporal variability in the ratio of trace gases emitted from biomass burning. Atmos. Chem. Phys., 11, 3611-3629, 2011.

Lefer, B. L., Talbot, R. W., Harriss, R. C., Bradshaw, J. D., Sandholm, S. T., Olson, J. O., Sachse, G. W., Collins, J., Shipman, M. A., Blake, D. R., Klemm, K. I., Gorzelska, K., and Barrick, J.: Enhancement of acidic gases in biomass burning impacted air masses over Canada, J. Geophys. Res. 99, 1721–1737, doi: 10.1029/93JD02091, 1994.

Leighton, P.: The Photochemistry of Air Pollution, Academic Press, 1961.

Liu, X., Huey, L. G., Yokelson, R. J., Selimovic, V., Simpson, I. J., Müller, M., Jimenez, J. L., Campuzano-Jost, P., Beyersdorf, A. J., Blake, D. R., Butterfield, Z., Choi, Y., Crounse, J. D., Day, D. A., Diskin, G. S., Dubey, M. K., Fortner, E., Hanisco, T. F., Hu, W., King, L. E., Kleinman, L., Meinardi, S., Mikoviny, T., Onasch, T. B., Palm, B. B., Peischl, J., Pollack, I. B., Ryerson, T. B., Sachse, G. W., Sedlacek, A. J., Shilling, J. E., Springston, S., St. Clair, J. M., Tanner, D. J., Teng, A. P., Wennberg, P. O., Wisthaler, A., and G. M. Wolfe.: Airborne measurements of western U.S. wildfire emissions: comparison with prescribed burning and air quality implications, J. Geophys. Res.-Atmos., 122, 6108–6129, https://doi.org/10.1002/2016JD026315, 2017.

McKeen, S. A., Liu, S. C., Hydrocarbon ratios and photochemical history of air masses, Geophys. Res. Lett., http://dx.doi.org/10.1029/93GL02527, 1984.

McKeen, S.A., Liu, S.C., Hsie, E.-Y., Lin, X.. Bradshaw, J.D., Smyth, S., Gregory, G.L., and Blake , D.R.: Hydrocarbon ratios during PEM-WEST A: A model perspective, J. Geophys. Res., 101, 2087–2109, doi: 10.1029/95JD02733, 1996.

Morton, B. R., G. I. Taylor, and J. S. Turner, 1956: Turbulent gravitational convection from maintained and instantaneous sources. Proc. Roy. Soc. London, A234,1-23.

Poppe, D., Koppmann, R. and Rudolph, J.: Ozone formation in biomass burning plumes: Influence of atmospheric dilution, Geophys. Res. Lett., 25, 3823–3826, 1998.

National Research Council: Estimating Mortality Risk Reduction and Economic Benefits from Controlling Ozone Air Pollution. National Academies Press, Washington D.C., 2008.

Pfister, G. G., Avise, J., Wiedinmyer, C., Edwards, D. P., Emmons, L. K., Diskin, G. D., Podolske, J., and Wisthaler, A.: CO source contribution analysis for California during ARCTAS-CARB, Atmos. Chem. Phys., 11, 7515-7532, https://doi.org/10.5194/acp-11-7515-2011, 2011.

Pinheiro, J.C., and Bates, D.M.: Mixed-Effects Models in S and S-PLUS, Springer, New York, 2000.

Reid, J. S., Koppmann, R., Eck, T. F., and Eleuterio, D. P.: A review of biomass burning emissions part II: intensive physical properties of biomass burning particles, Atmos. Chem. Phys., 5, 799-825, https://doi.org/10.5194/acp-5-799-2005, 2005.

Roberts, J. M., F. C. Fehsenfeld, S. C. Liu, M. J. Bollinger, C. Hahn, D. L. Albritton, and R. E. Sievers: Measurements of aromatic hydrocarbon ratios and NOx concentrations in the rural troposphere: Estimates of air mass photochemical age and NOx removal rate, Atmos. Environ., 18, 2421–2432, 1984.

Ryerson, T. B., Williams, E. J., and Fehsenfeld, F.C.: An efficient photolysis system for fast-response NO_2 measurements, J. Geophys. Res.-Atmos., doi:10.1029/2000JD900389, 2000.

Seinfeld, J.H. and S.N. Pandis, Atmospheric Chemistry and Physics: From Air Pollution to Climate Change, 3rd Edition, Wiley, 2016.

Simpson, I. J., Akagi, S. K., Barletta, B., Blake, N. J., Choi, Y., Diskin, G. S., Fried, A., Fuelberg, H. E., Meinardi, S., Rowland, F. S., Vay, S. A., Weinheimer, A. J., Wennberg, P. O., Wiebring, P., Wisthaler, A., Yang, M., Yokelson, R. J., and Blake, D. R.: Boreal forest fire emissions in fresh Canadian smoke plumes: C1-C10 volatile organic compounds (VOCs), CO2, CO, NO2, NO, HCN and CH3CN, Atmos. Chem. Phys., 11, 6445-6463, https://doi.org/10.5194/acp-11-6445-2011, 2011.

Singh, H. B., and the ARCTAS Science Team: Pollution influences on atmospheric composition and chemistry at high northern latitudes: Boreal and California forest fire emissions, Atmos. Environ., 44, 4553-4564, 2010.

Singh, H. B., Cai, C., Kaduwela, A., Weinheimer, A., and Wisthaler, A.: Interactions of fire emissions and urban pollution over California: Ozone formation and air quality simulations, Atmos. Environ., 56, 2, 45-51, 2012.

Squires, P. and Turner, J.S.: An entraining jet model for cumulo-nimbus updraughts. Tellus A. 10.3402/tellus.v14i4.9569.1962.

Toon, O. B., Maring, H., Dibb, J., Ferrare, R., Jacob, D. J., Jensen, E. J., Luo, Z. J., Mace, G. G., Pan, L. L., Pfister, L., Rosenlof, K. H., Redemann, J., Reid, J. S., Singh, H. B., Thompson, A. M., Yokelson, R., Minnis, P., Chen, G., Jucks, K. W., Pszenny A.: Planning, implementation and scientific goals of the Studies of Emissions and Atmospheric Composition, Clouds and Climate Coupling by Regional Surveys (SEAC4RS) field mission, J. Geophys. Res. – Atmos., 121, 4967-5009, doi:10.1002/2015JD024297, 2016.

Trenberth, K.: Some effects of finite sample size and persistence on meteorological statistics. Part I: Autocorrelations, Monthly Weather Review, 112, 2359–2368, 1984.

Trentmann, J., Andreae, M. O., Graf, H.-F., Hobbs, P. V., Ottmar, R. D., and Trautmann, T.: Simulation of a biomass burning plume: Comparison of model results with observations: J. Geophys. Res., 107, 4013, doi:10.1029/2001JD000410, 2002.

U.S. EPA: U.S. Environmental Protection Agency 2002 National Emissions Inventory. Available: http://www.epa.gov/ttn/chief/net/2002invent, 2006.

Wagner, N. L., Brock, C. A., Angevine, W. M., Beyersdorf, A., Campuzano-Jost, P., Day, D., de Gouw, J. A., Diskin, G. S., Gordon, T. D., Graus, M. G., Holloway, J. S., Huey, G., Jimenez, J. L., Lack, D. A., Liao, J., Liu, X., Markovic, M. Z., Middlebrook, A. M., Mikoviny, T., Peischl, J., Perring, A. E., Richardson, M. S., Ryerson, T. B., Schwarz, J. P., Warneke, C., Welti, A., Wisthaler, A., Ziemba, L. D., and Murphy, D. M.: In situ vertical profiles of aerosol extinction, mass, and composition over the southeast United States during SENEX and SEAC^{4}RS: observations of a modest aerosol enhancement aloft, Atmos. Chem. Phys., 15, 7085-7102, https://doi.org/10.5194/acp-15-7085-2015, 2015.

Warneke, C., de Gouw, J. A., Edwards, P. M., Holloway, J. S., Gilman, J. B., Kuster, W. C., Graus, M., Atlas, E., Blake, D., Gentner, D. R., Goldstein, A. H., Harley, R. A., Alvarez, S., Rappenglueck, B., Trainer, M., and Parrish, D. D.: Photochemical aging of volatile organic compounds in the Los Angeles basin: Weekday-weekend effect, J. Geophys. Res.-Atmos., 118, 5018–5028, https://doi.org/10.1002/jgrd.50423, 2013.

Weinheimer, A. J., Walega, J. G., Ridley, B. A., Gary, B. L., Blake, D. R., Blake, N. J., Rowland, F. S., Sachse, G. W., Anderson, B. E., and Collins, J. E.: Meridional distributions of NOx, NOy, and other species in the lower stratosphere and upper troposphere during AASE II, Geophys. Res. Lett., 21, 2583–2586, 1994.

Wang, H.: Formation of nascent soot and other condensed-phase materials in flames: Proceedings of the Combustion Institute, 33, 41-67, doi:10.1016/j.proci.2010.09.009, 2011.

Wilkinson Graham N. , Rogers CE (1973). "Symbolic Description of Factorial Models for Analysis of Variance." Applied Statistics, 22, 392–399.

Wilson, E. B., First and second laws of error. Journal of the American Statistical Association 18 841-851, 1923.

Wisthaler, Armin; Crawford, J.H; Haidahcer, S.; Hanel, G.; Hartungen, E.; Jordan, A.; Märk, L.; Mikoviny, T.; Müller, M.; Mutschlechner, P.; Schottkowsky, R. & Sulzer: Development of a compact PTR-ToF-MS for suborbital research on the earth's atmospheric composition, In A Hansel & J. Dunkel (ed.), 6th International Conference on Proton Transfer Reaction Mass Spectrometry and its Applications. Contributions. Innsbruck University Press. ISBN 978-3902811912. pp 96 – 96, 2013.

Yates, E.L., Schiro, K., Lowenstein, M., Sheffner, E.J., Iraci, L.T., Tadić, J.M.; Kuze, A: Carbon Dioxide and Methane at a Desert Site—A Case Study at Railroad Valley Playa, Nevada, USA. Atmosphere 2011, 2, 702-714.

Yokelson, R.J., D.W.T. Griffith, and D.E. Ward: Open-path Fourier transform infrared studies of large-scale laboratory biomass fires, J. Geophys. Res., 101, 21067021080,11996, 1996.

Yokelson, R. J., Karl, T., Artaxo, P., Blake, D. R., Christian, T. J., Griffith, D. W. T., Guenther, A., and Hao, W. M.: The Tropical Forest and Fire Emissions Experiment: overview and airborne fire emission factor measurements, Atmos. Chem. Phys., 7, 5175-5196, https://doi.org/10.5194/acp-7-5175-2007, 2007.

Yokelson, R.J., M. O. Andreae, and S. K. Akagi, Pitfalls with the use of enhancement ratios or normalized excess mixing ratios measured in plumes to characterize pollutant sources and aging Atmos. Meas. Tech., 6, 2155–2158, 2013.

Vay, S. A., Choi, Y., Vadrevu, K. P., Blake, D. R., Tyler, S. C., Wisthaler, A., Hecobian, A., Kondo, Y., Diskin, G. S., Sachse, G. W., Woo, J.-H., Weinheimer, A. J., Burkhart, J. F., Stohl, A., Wennberg, P. O.: Patterns of CO2 and radiocarbon across high northern latitudes during IPY 2008, J. Geophys. Res., 116, doi:10.1029/2011JD015643, 2011.